AGU PUBLICATIONS

Space Weather

RESEARCH ARTICLE
10.1002/2016SW001407

Special Section:
Initial Results from the NASA Radiation Dosimetry Experiment (RaD-X) Balloon Flight Mission

Cosmic radiation dose measurements from the RaD-X flight campaign

Christopher J. Mertens[1], Guillaume P. Gronoff[2], Ryan B. Norman[1], Bryan M. Hayes[1,3], Terry C. Lusby[4], Tore Straume[4], W. Kent Tobiska[5], Alex Hands[6], Keith Ryden[6], Eric Benton[3], Scott Wiley[7], Brad Gersey[8], Richard Wilkins[8], and Xiaojing Xu[9]

[1]NASA Langley Research Center, Hampton, Virginia, USA, [2]Science Systems and Applications, Inc., Hampton, Virginia, USA, [3]Department of Physics, Oklahoma State University, Stillwater, Oklahoma, USA, [4]NASA Ames Research Center, Moffett Field, California, USA, [5]Space Environment Technologies, Los Angeles, California, USA, [6]Surrey Space Center, University of Surrey, Guildford, UK, [7]Jacobs Technology, Inc., Edwards, California, USA, [8]Department of Electrical and Computer Engineering, Prairie View A&M University, Prairie View, Texas, USA, [9]National Institute of Aerospace, Hampton, Virginia, USA

Key Points:
- The RaD-X campaign provided dosimetric measurement at seven altitudes from 8 km to over 32 km
- Flight-averaged absorbed dose rates measured by the TEPC, Liulin, and Teledyne detectors agree to within 15% in stratosphere
- The balloon flight data show the absence of a distinct Pfotzermaximum in the dose equivalent rate

Correspondence to:
C. J. Mertens,
Christopher.J.Mertens@nasa.gov

Citation:
Mertens, C. J., et al. (2016), Cosmic radiation dose measurements from the RaD-X flight campaign, *Space Weather*, *14*, 874–898, doi:10.1002/2016SW001407.

Received 21 APR 2016
Accepted 28 SEP 2016
Accepted article online 6 OCT 2016
Published online 28 OCT 2016

©2016. American Geophysical Union. All Rights Reserved.

Abstract The NASA Radiation Dosimetry Experiment (RaD-X) stratospheric balloon flight mission obtained measurements for improving the understanding of cosmic radiation transport in the atmosphere and human exposure to this ionizing radiation field in the aircraft environment. The value of dosimetric measurements from the balloon platform is that they can be used to characterize cosmic ray primaries, the ultimate source of aviation radiation exposure. In addition, radiation detectors were flown to assess their potential application to long-term, continuous monitoring of the aircraft radiation environment. The RaD-X balloon was successfully launched from Fort Sumner, New Mexico (34.5°N, 104.2°W) on 25 September 2015. Over 18 h of flight data were obtained from each of the four different science instruments at altitudes above 20 km. The RaD-X balloon flight was supplemented by contemporaneous aircraft measurements. Flight-averaged dosimetric quantities are reported at seven altitudes to provide benchmark measurements for improving aviation radiation models. The altitude range of the flight data extends from commercial aircraft altitudes to above the Pfotzer maximum where the dosimetric quantities are influenced by cosmic ray primaries. The RaD-X balloon flight observed an absence of the Pfotzer maximum in the measurements of dose equivalent rate.

1. Introduction

The Radiation Dosimetry Experiment (RaD-X) flight mission was funded by the NASA Science Mission Directorate under the Hands-On Project Experience (HOPE)-4 opportunity. The purpose of the HOPE opportunity is to provide early career engineers with full-cycle flight project experience via a short-duration, low-cost flight mission. Within these funding and schedule constraints, the RaD-X flight mission was designed with low-cost, available dosimeters to take high-altitude measurements that can be used to improve the understanding of cosmic radiation transport in the atmosphere and the subsequent radiation exposure to passengers and aircrew in the aircraft environment. The value of the RaD-X flight campaign to the aviation radiation community is the following. One, balloon flight dosimetric measurements were taken at high altitudes from four different type dosimeters, at an altitude region where measurement data are relatively sparse. Two, the flight measurements were taken at a geomagnetic cutoff rigidity where aviation radiation model uncertainty is near its peak. Third, the high-quality benchmark measurements of flight-averaged dosimetric quantities can, in principle, lead to a reduction in model uncertainty by nearly a factor of 2 for geomagnetic vertical cutoff rigidities (hereafter referred to as simply cutoff rigidity) of ~4 GV or greater. And fourth, the RaD-X science payload can be flown on future balloon missions or dedicated aircraft experiments with minimal development cost.

There are two sources of cosmic radiation: (1) the ever present galactic cosmic rays (GCR), which originate from outside the solar system [e.g., *Gaisser*, 1990] and (2) the transient solar energetic particles (SEP) (or solar cosmic rays), which are produced by eruptions on the Sun's surface, with event durations lasting from hours to days [e.g., *Gopalswamy et al.*, 2006]. Cosmic rays are comprised of high-energy charged particles that can penetrate deep within the atmosphere, producing the single most important source to human radiation exposure at aircraft altitudes. The high-LET (linear energy transfer) quality of cosmic radiation increases its potential to

modify healthy tissue cells, thereby increasing the risk of cancer development or other harmful health effects [*Wilson et al.*, 2003, 2005]. Adverse reproductive outcomes have been suggested in some studies of female flight attendants [*Aspholm et al.*, 1999; *Lauria et al.*, 2006; *Waters et al.*, 2000]. Also, a 70% increase in the risk of miscarriage among flight attendants, who received a dose of 0.1 mGy (1 Gy = J/kg) or more in the first trimester, was shown in a recent epidemiological study [*Grajewski et al.*, 2015].

Commercial aircrews are classified as radiation workers by the International Commission on Radiobiological Protection (ICRP) [*International Commission on Radiobiological Protection (ICRP)*, 1991]. This designation is accepted by most countries, including the United States (U.S.), Canada, and the European Union (EU) [*National Council on Radiation Protection and Measurements (NCRP)*, 2009; *Lindborg et al.*, 2004]. The U.S. National Council on Radiation Protection and Measurements (NCRP) found that crews of commercial aircraft received the largest effective dose compared to other terrestrial radiation workers monitored during the same study period [*NCRP*, 2009]. Nevertheless, U.S. aircrews represent an occupational group exposed to undocumented and unquantified radiation levels over the duration of their careers. In addition, the current ICRP guidelines for maximum prenatal and public exposures can be exceeded during a single solar storm event for passengers on cross-polar or intercontinental commercial routes, or by frequent use (~5–10 round-trip flights per year) of these high-latitude routes even during quiet solar conditions, in the absence of SEP events [*American Meterological Society*, 2007; *Copeland et al.*, 2008; *Dyer et al.*, 2009; *Mertens et al.*, 2012].

The RaD-X mission obtained dosimetric measurements for understanding the transport of cosmic radiation and human exposure to this radiation field at aircraft altitudes. The first science goal of the RaD-X mission is to provide measurements that will help characterize the dosimetric properties of cosmic ray primary particles, which are the ultimate source of radiation exposure at aviation altitudes. These measurements can be used to improve aviation radiation models by providing observations to assist the evaluation of model uncertainty in predicting cosmic ray primaries and the subsequent propagation of this uncertainty in predicting radiation exposure at aircraft altitudes. The second RaD-X science goal is to assess the feasibility of specific compact radiation detectors as potential technologies for long-term, continuous monitoring of the aircraft radiation environment. A more detailed discussion of the background and motivation for the RaD-X science mission goals is given in the overview of this special issue [*Mertens*, this issue].

The RaD-X campaign consists of the primary stratospheric balloon flight, supplemented by four supporting aircraft flights. The RaD-X balloon was launched on 25 September 2015 from Fort Sumner, New Mexico (34.5°N, 104.2°W). The geomagnetic cutoff rigidity at Fort Sumner is approximately 4 GV. Dosimetric measurements at this location are advantageous for fostering aviation radiation model improvements, since the relative data spread in comparisons of the calculated aircraft radiation dose among 11 models for GCR exposures increases from 20% at low-cutoff rigidities and high latitudes to nearly 50% at high-cutoff rigidities and low latitudes [*Bottollier-Depois et al.*, 2012]. Furthermore, the Nowcast of Atmospheric Ionizing Radiation for Aviation Safety (NAIRAS) model predictions of ambient dose equivalent rate are generally within 10% of aircraft flight measurements at high latitudes and low-cutoff rigidities, with differences increasing to 50% for cutoff rigidities at roughly 4 GV and higher [*Mertens et al.*, 2013]. The recommended criterion on the uncertainty of dose assessments at aviation altitudes is that the total relative standard uncertainty not exceed 30% for ambient dose equivalent equal to or greater than an annual exposure of 1 mSv [*International Commission on Radiation Units (ICRU)*, 2010]. Using a conservative estimate of pilot annual block hours, *Mertens et al.* [2013] concluded that aircraft dose assessments should be within the International Commission on Radiation Units (ICRU) uncertainty criterion for locations with geomagnetic cutoff rigidity less than ~10 GV. Based on manufacturer-reported accuracies and the laboratory exposures conducted by *Straume et al.* [2016], and the statistical uncertainty of the RaD-X campaign flights (<5%), the total standard uncertainty of the RaD-X flight-averaged dosimetric quantities are less than 30%. In principle, the RaD-X measurements can lead to a reduction in the region of maximum model uncertainty in the prediction of the radiation protection quantities by nearly a factor of 2.

The RaD-X balloon payload consists of four science instruments. The primary science instrument is a tissue equivalent proportional counter (TEPC) microdosimeter, which measures the LET spectrum in an equivalent spherical tissue volume of 2 μm in diameter [*Conroy*, 2010]. The dosimetric quantities utilized in radiation protection are derived for the RaD-X balloon flight from the TEPC's fundamental measurement of the tissue equivalent LET spectrum [*Conroy*, 2010; *Lillhök et al.*, 2007; *Silari et al.*, 2009]. The second science instrument is the Liulin dosimeter-spectrometer [*Dachev et al.*, 2015]. Liulin measurements of energy deposition spectra

in silicon are combined with TEPC measurements to characterize the dosimetric properties of cosmic ray primaries in the analysis of the RaD-X flight data. The silicon-based Teledyne total ionizing dose (TID) and RaySure detectors aboard the balloon payload are candidate technologies for the application of continuous, long-term monitoring of the aircraft radiation environment [*Mazur et al.*, 2011; *Dyer et al.*, 2009; *Hands and Dyer*, 2009]. The initial assessment of the TID and RaySure detectors conducted by the RaD-X mission is based on their consistency with the Liulin and TEPC dosimetric measurements, respectively, during the laboratory radiation source exposures [*Straume et al.*, 2016] and during the balloon flight. For brevity, the three silicon-based detectors will be referred to as Liulin, TID, and RaySure hereafter.

One of the fundamental differences between the TEPC and the silicon detectors is their response to neutrons. This is particularly important for the neutron-rich atmospheric radiation environment where neutrons dominate the radiobiological dosimetric quantities at aviation altitudes [e.g., *Copeland*, 2014; *Mertens et al.*, 2012; *Lindborg et al.*, 2004]. The TEPC responds to neutrons through indirect ionization by recoil protons produced in the tissue equivalent plastic wall of the detector cavity by nuclear collisions with the incident neutrons [*ICRU*, 1983]. Silicon detectors also respond to neutrons by indirect ionization. But in this case, the secondary ionizing particles also include recoil silicon nuclei as well as protons and alpha particles from inelastic nuclear interactions between incident neutrons and silicon [*Hands and Dyer*, 2009]. The purpose of instrument calibration is to ensure that the correct dosimetric quantity is derived from the measurement, given an instrument's particular response to the radiation environment. For example, the RaySure is calibrated to measure dose equivalent in good agreement with TEPC measurements at aviation altitudes [*Hands and Dyer*, 2009], despite the differences in measurement technique and neutron response between the two instruments. The challenge of interpreting the differences between dosimeter measurements in the space and atmospheric radiation environments is that these environments can not be fully reproduced in the laboratory. A cautionary stance must be taken. There is always the possibility that the agreement between two different dosimeters in the complex atmospheric or space radiation environment is due to a fortuitous cancelation of errors.

The RaD-X balloon flight collected 20 h of science data. Over 18 h of the flight time was above the Pfotzer maximum, at barometric altitudes greater than 20 km. These altitudes, combined with the dosimeter and spectrometer instruments, provide a unique measurement data set for improving aviation radiation models. The dose and spectral measurements above the Pfotzer maximum facilitate the characterization of the source of cosmic radiation exposure at aviation altitudes [*Mertens*, this issue]. The balloon flight trajectory near Fort Sumner is located at cutoff rigidities where aviation radiation model uncertainty is near its maximum [*Bottollier-Depois et al.*, 2012].

The RaD-X balloon flight utilized the natural descent of the balloon after sunset to obtain measurements in two altitude regions. The highest altitude region, hereafter referred to as Region B, was defined by barometric altitudes greater than 32 km. In Region B, the contributions from heavy-ion cosmic ray primaries are discernible in the dosimetric measurements. After sunset, the balloon descended in altitude and was maintained in the barometric altitude region 21–27 km, hereafter referred to as Region A, by adjusting the ballast on the balloon gondola. The contributions of cosmic ray primaries to the dosimetric measurements in Region A are almost exclusively due to protons. Thus, these two altitude regions exploit the function of the atmosphere as a natural cosmic radiation spectral analyzer, by using the altitude of the atmosphere to separately identify the dosimetric contributions from cosmic ray primary protons, the most abundant component of the primary cosmic ray spectrum, and the heavy-ion contributions, which are also a rich source of secondary radiation transported to aircraft altitudes.

The four supporting aircraft flights provided significant scientific enhancement to the RaD-X balloon flight measurements. Two of the aircraft flights were nearly spatially-temporally coincident with the RaD-X balloon flight trajectory. On 9 September 2015, the NASA Armstrong Flight Research Center (AFRC) flew an ER-2 aircraft in the vicinity of Fort Sumner, providing TEPC dosimetric measurements at two primary cruise (barometric) altitudes, 20 km and 17 km. The Upper atmospheric Space and Earth Weather eXperiment (USEWX) project equipped the ER-2 aircraft with the TEPC instrument. The highest cruise altitude (20 km) is near the Pfotzer maximum where the peak in secondary particle production occurs. The lower cruise altitude (17 km) is at the bottom side of the Pfotzer maximum and corresponds to an altitude region where attenuation processes dominate over particle production. A Cessna Conquest II aircraft, operated by Columbia Scientific Balloon Facility (CSBF), took dosimetric measurements in an area around Fort Sumner on 27 September 2015.

The CSBF aircraft was equipped with a Liulin and two TEPCs. The cruise altitude was (geodetic) 8 km, which is representative of the low-altitude end of commercial aircraft flight levels. The German Aerospace Center (DLR) conducted a flight campaign in support of the RaD-X mission which consisted of dosimetric measurements from a TEPC and a Liulin on two Lufthansa German Airlines commercial flights [*Meier et al.*, 2016]. The two flights occurred on 12 and 15 September 2015 at geomagnetic cutoff rigidities similar to the RaD-X balloon flight and at barometric cruise altitudes of 11.3 km and 10.4 km, respectively.

The RaD-X campaign, in total, provided dosimetric measurements at seven altitudes, corresponding to atmospheric regions defined by distinctly different transport and collisional interaction physics. The four different-type radiation instruments used in the RaD-X campaign facilitate complementary ways of analyzing the flight data, as shown in section 5, and enable in-field instrument intercomparisons at several altitude regions with distinctly different cosmic radiation environment characteristics. The balloon and aircraft flights were conducted under solar and geomagnetically quiet conditions, which was expected at the geomagnetic cutoff rigidities of these flights. Most of the flight measurements were obtained at nearly the same geomagnetic cutoff rigidity, enabling a significant reduction in statistical uncertainty. Moreover, the cutoff rigidity around the Fort Sumner area is at a value where model uncertainty is near its peak [*Bottollier-Depois et al.*, 2012]. Therefore, the RaD-X campaign produced a unique dosimetry data set for investigating the physics of cosmic radiation transport in the atmosphere and for improving the assessment of radiation exposure at aviation altitudes.

The remainder of the paper is organized as follows. The dosimetric quantities obtained from the RaD-X campaign flight measurements are introduced and defined in section 2. A brief description of the science instruments is given in section 3. Section 4 summarizes the balloon and aircraft flight profiles. The flight results are presented and discussed in section 5. Section 6 contains the summary and conclusions.

2. Dosimetric Quantities

The dosimetric quantities measured during the RaD-X campaign are absorbed dose in tissue and in silicon, dose equivalent, ambient dose equivalent, LET spectral dose distribution in tissue, and energy deposition spectra in silicon. The instruments used to obtain these quantities during the RaD-X campaign are discussed in the next section.

The definitions of the fundamental dosimetric quantities are as follows. Absorbed dose is defined as the energy deposited per mass in a target medium by the radiation field. The SI unit for absorbed dose is the Gray (1 Gy = J/kg). The dose equivalent quantity folds the spectral dose distribution in tissue with a LET-dependent quality factor ($Q(L)$), which accounts for the relative effectiveness of the radiation field in producing biological damage [*ICRP*, 2007]. The SI unit for dose equivalent is the Sievert (Sv). Ambient dose equivalent, denoted $H^*(10)$, is an operational quantity introduced by the ICRP/ICRU for radiation protection applications [*ICRP*, 2007; *ICRU*, 2010]. In practice, $H^*(10)$ is a reasonable operational proxy related to the total biological detriment to the human body. The SI unit for $H^*(10)$ is also the Sievert (Sv).

3. Science Instruments

The four science instruments on the RaD-X balloon payload are shown in Figure 1. The manufacturer, model number, and dosimetric quantities analyzed for each of the balloon payload instruments are listed in Table 1. Brief descriptions of the balloon payload instruments are presented in section 3.1. Table 2 lists the instruments and dosimetric quantities analyzed from the supporting aircraft flights with a description of the aircraft payloads given in section 3.2.

3.1. Balloon Payload

The TEPC is the de facto instrument in microdosimetry [*ICRU*, 1983, 2010]. The TEPC flown on the balloon flight was a Hawk version 3.0, manufactured by Far West Technologies (FWT), Inc. The Liulin dosimeter-spectrometer was manufactured by the Space Research and Technology Institute (SRTI) of the Bulgarian Academy of Sciences. The model flown on the balloon flight was the Liulin-6SA Mobile Dosimetry Unit (MDU). The RaD-X-designated total ionizing dose (TID) detector is the μDOS commercial class (UDOS001-C) dosimeter manufactured by Teledyne Microelectronic Technologies. The RaySure detector, provided by the University

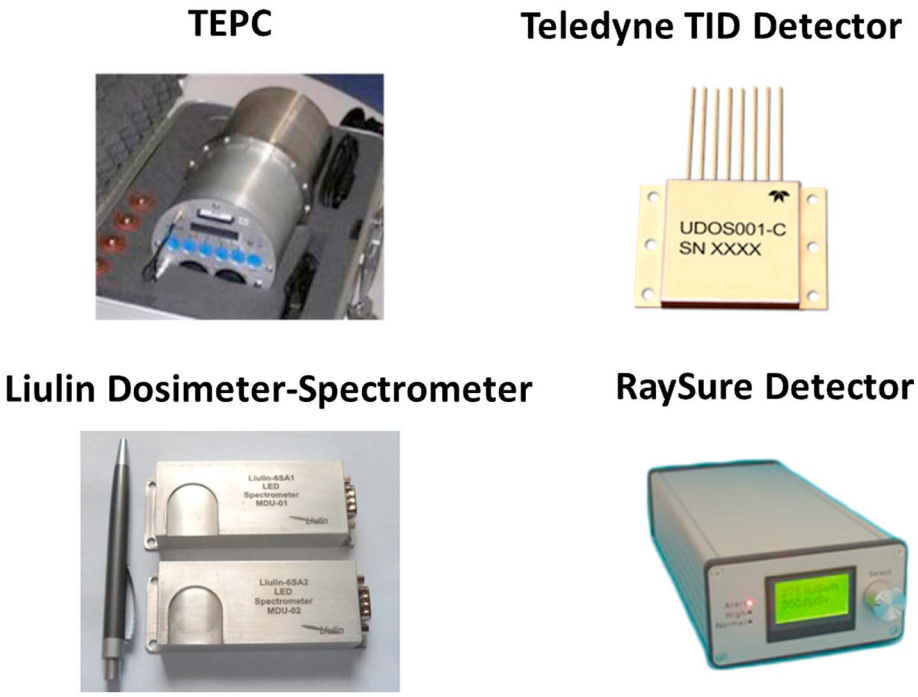

Figure 1. RaD-X balloon payload science instruments. The TEPC is in a padded case the size of carry-on luggage. The Liulin is roughly the size of an iPod nano. The TID detector is thumb size. The RaySure detector is about the size of a typical bench digital multimeter. The relative size of the instruments can be seen in Figure 2.

of Surrey, United Kingdom (UK), is a compact radiation sensor originally designed for use in aircraft. A power and thermal interface was designed to integrate the RaySure to the balloon payload. The four RaD-X balloon payload instruments are discussed in more detail in an article included in this special issue that presents the ground testing and calibration of the payload instruments [*Straume et al.*, 2016].

Table 1. RaD-X Balloon Payload Science Instruments and Measurement Quantities

Instrument	Manufacturer	Model	Measurement Quantities
TEPC	FWT	Hawk 3.0	Absorbed dose rate (μGy/h)
			Dose equivalent rate (μSv/h)
			Ambient dose equivalent rate (μSv/h)[a]
			LET spectrum: 0.3–1500 keV/μm
Liulin	SRTI	Liulin-6SA	Absorbed dose rate (μGy/h)
			Energy deposition spectrum: 0.1–20.8 MeV
			(or LET spectrum: 0.3–69.4 keV/μm)[b]
TID	Teledyne	μDOS001-C	Absorbed dose rate (μGy/h)[c]
			(Sensitive to energy deposits: 0.1–15 MeV)
			(or sensitive to LET: 0.4–60 keV/μm)[b]
RaySure	QinetiQ	Version 3B	Absorbed dose rate (μGy/h)
			Dose equivalent rate (μSv/h)
			Energy deposition spectrum: 0.1–100 MeV
			(or LET spectrum: 0.2–200 keV/μm)[b]

[a]H*(10) derived from measured LET spectrum combined with Low-LET/High-LET calibration coefficients—see *Straume et al.* [2016].

[b]LET approximated for silicon detectors by dividing the energy deposited by the thickness of the detector disk.

[c]Instrument measures accumulated dose. Dose rate computed via numerical differentiation of accumulated dose.

Table 2. RaD-X Supporting Aircraft Science Instruments and Measurement Quantities

Aircraft	Instrument	Manufacturer	Model	Measurement Quantities
ER-2	TEPC	FWT	Hawk 2.0	Absorbed dose rate (μGy/h)
				Dose equivalent rate (μSv/h)
				LET spectrum: 0.3–1000 keV/μm
CSBF[a]	TEPC	FWT	Hawk 3.0	Absorbed dose rate (μGy/h)
				Dose equivalent rate (μSv/h)
				LET spectrum: 0.3–1500 keV/μm
	TEPC	FWT	Hawk 2.0	Absorbed dose rate (μGy/h)
				Dose equivalent rate (μSv/h)
				LET spectrum: 0.3–1000 keV/μ
	Liulin	SRTI	Liulin-4U	Absorbed dose rate (μGy/h)
				Energy deposition spectrum: 0.1–20.8 MeV
				(or LET spectrum: 0.3–69.4 keV/μm)
DLR[b]	TEPC	FWT	Hawk 2.0	Absorbed dose rate (μGy/h)
				Dose equivalent rate (μSv/h)
				LET spectrum: 0.3–1000 keV/μ
	Liulin	SRTI	Liulin-6G	Absorbed dose rate (μGy/h)
				Energy deposition spectrum: 0.1–20.8 MeV
				(or LET spectrum: 0.3–69.4 keV/μm)

[a]CSBF chase plane is a Cessna Conquest II aircraft.
[b]The DLR flights were on Lufthansa commercial aircraft.

3.2. Aircraft Payloads

The aircraft instrument payloads consisted of a subset of the balloon instruments. The NASA AFRC ER-2 aircraft was equipped with a Hawk version 2.0 TEPC. The TEPC was provided by SolarMetrics, UK, and integrated to the ER-2 aircraft by the AFRC's USEWX project. The TEPC was placed in a sealed aluminum container and pressurized to 1013 hPa (1 atm) of dry air.

The CSBF aircraft was equipped with both a Hawk version 2.0 and a Hawk version 3.0 TEPC, and a Liulin-4 MDU dosimeter-spectrometer [*Dachev et al.*, 2002; *Dachev*, 2009]. The Hawk version 3.0 TEPC was the RaD-X balloon flight spare. The Hawk version 2.0 TEPC and the Liulin-4 MDU were provided by Oklahoma State University (OSU).

The Lufthansa commercial aircraft that participated in the DLR flight campaign included a Hawk version 2.0 TEPC and Liulin-6G MDU [*Meier et al.*, 2016].

4. Flight Profiles

4.1. Balloon Payload

All altitudes referenced in this section are barometric altitudes, which are defined in terms of the pressure levels of the U.S. Standard Atmosphere.

The balloon science payload is shown in Figure 2. The TEPC and RaySure instruments were sealed in aluminum containers and pressurized to 1013 hPa (1 atm) of dry nitrogen gas. Prior to launch, the science payload was covered with 5.1 cm (2 inches) thick polyethylene foam for thermal protection and integrated to the CSBF balloon gondola. The gondola also contains the batteries and the Communications Interface Package (CIP). The CIP includes a RF data link to command and control the balloon operations, and to provide GPS tracking and pressure-altitude information during the flight. The RaD-X science and engineering data were transmitted to the CSBF Flight Operations Center at Fort Sumner via the CIP. RaD-X data were also stored on board the flight computer.

The RaD-X balloon flight mission was launched at the NASA Balloon Program Office's Scientific Balloon Flight Facility, operated by CSBF, located in Fort Sumner, NM (34.5°N, 104.2°W) on 25 September 2015. The balloon itself was a 311,000 m^3 (11×10^6 ft^3) zero pressure balloon, partially filled with helium gas.

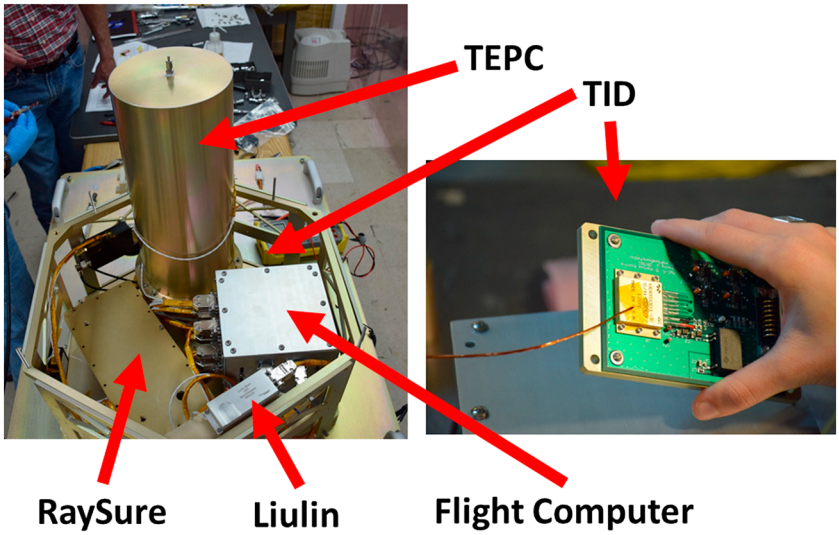

Figure 2. RaD-X science payload. The TEPC and RaySure detector are enclosed in aluminum containers pressured to one atmosphere of nitrogen. The TID detector is lying face up on the surface of the payload structure, behind the flight computer, and cannot be seen in the left photo. The TID board is shown in the right photo.

The main features of the flight profile of the RaD-X balloon are summarized in Figure 3. The science payload was powered on at 11:20 UTC (05:20 MDT) on 25 September 2015. The balloon was launched at 17:06 UTC (11:06 MDT) and ascended for 1.74 h until it reached science Region B at 18:50 UTC (12:50 MDT), which is defined as altitudes greater than 32.5 km, or pressure levels less than 8 hPa. The balloon spent 6.65 h in Region B. The balloon began to slowly descend in altitude at 20:37 UTC (14:37 MDT) and exited Region B at 01:29 UTC (19:37 MDT).

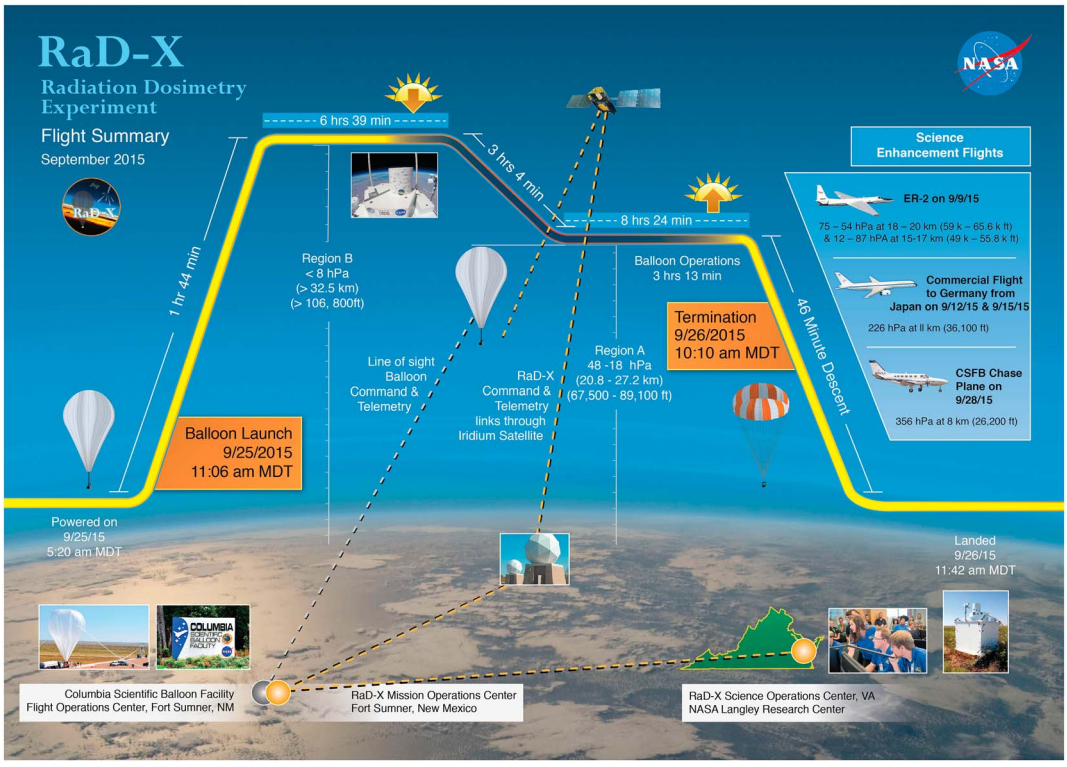

Figure 3. RaD-X balloon flight profile summary. The altitudes are defined as barometric altitudes.

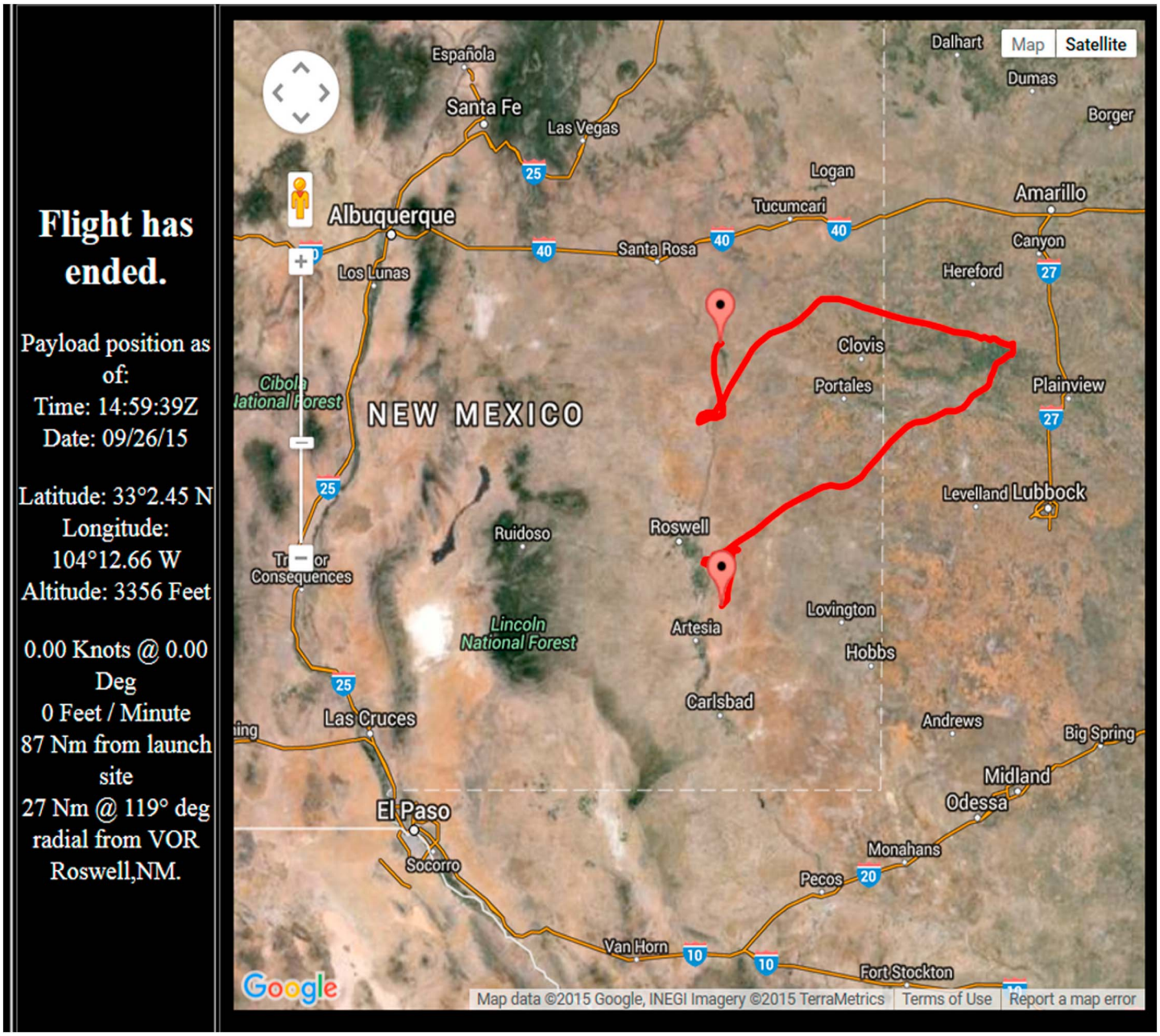

Figure 4. RaD-X balloon flight ground track.

At 04:33 UTC (22:33 MDT), the balloon entered science Region A, which is defined as the altitude region 21–27 km or pressure level region 18–48 hPa. The balloon remained in Region A for 8.4 h. At approximately 11:53 UTC (05:53 MDT), a ballast was dropped so that the upper stratospheric winds would steer the balloon over a sparsely populated region for mission termination. The balloon exited Region A at 12:56 UTC (07:56 MDT) as it ascended to higher altitudes. The RaD-X flight was terminated at 14:10 UTC (08:10 MDT) on 26 September 2015 with the balloon landing near Roswell, NM, approximately 46 min later. The ground track of the RaD-X balloon flight is shown in Figure 4.

Figure 5 shows the CIP measurements of altitude and pressure during the RaD-X balloon flight. The average altitude and pressure for the time spent in Region B are 36.7 km and 4.5 hPa, respectively. The highest altitude attained in Region B was 38.3 km, corresponding to 3.55 hPa, at 20:04 UTC (14:04 MDT). The average altitude

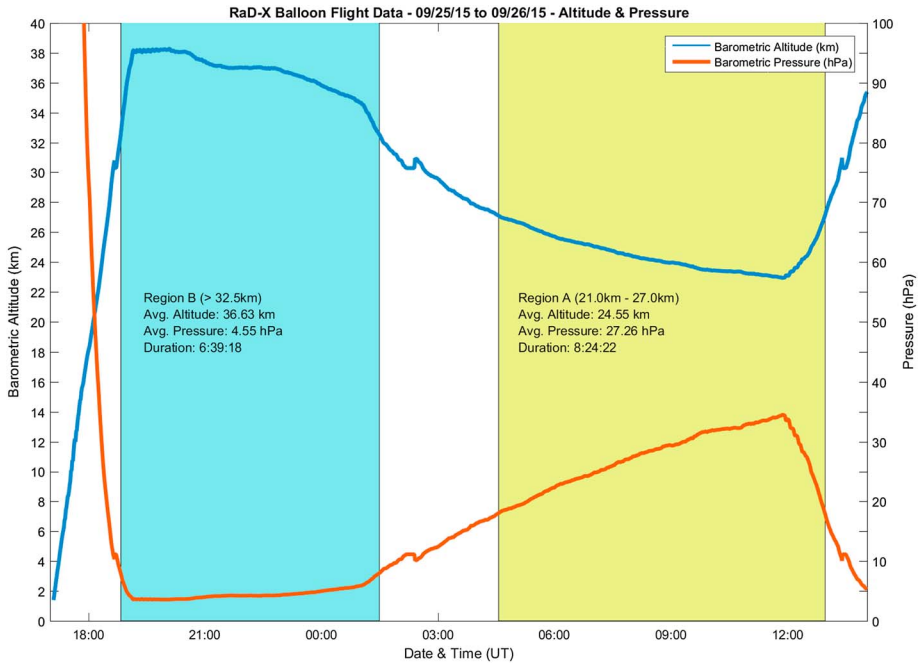

Figure 5. Barometric altitude and pressure measurements during the RaD-X balloon flight, provided by the CIP.

and pressure during the balloon passage through Region A are 24.5 km and 27.3 hPa, respectively. The lowest altitude reached in Region A was 22.9 km at 11:52 UTC (5:52 MDT), which corresponds to 34.5 hPa.

The RaD-X balloon flight was confined to a narrow range in geomagnetic cutoff rigidity. The average cutoff in Region A is 3.8 $\pm$ 0.1 GV, with a minimum and maximum of 3.6 GV and 4.0 GV, respectively. The minimum and maximum cutoffs in Region B are 3.4 GV and 3.8 GV, respectively. The average cutoff in Region B is 3.5 $\pm$ 0.1 GV. The cutoffs were calculated from the NAIRAS model [*Mertens et al.*, 2010], which uses the CISM-Dartmouth real-time geomagnetic cutoff code [*Kress et al.*, 2010].

4.2. ER-2 Aircraft

All altitudes referenced in this section are barometric altitudes.

The NASA AFRC's ER-2 took off from Palmdale United States Air Force (USAF) base, located in California (34.6°N, 118.1°W), on 9 September 2015 at 16:00 UTC (09:00 PDT). The aircraft reached an altitude of 17 km (FL550) at time 16:33 UTC and geographic coordinates 34.96°N, 116.58°W. The aircraft remained at this altitude for 2.75 h before ascending to a higher cruise altitude. The geographic location just prior to the altitude ascent was 34.49°N, 98.67°W. The aircraft reached an altitude of 20 km (FL650) at time 19:18 UTC and geographic location 34.71°N, 104.20°W. The aircraft remained at this altitude for 1.4 h. The altitude descent began at the location 34.70°N, 112.48°W before returning to Palmdale USAF base.

The variation in geomagnetic cutoff rigidity over the ER-2 flight path is described as follows. The average cutoff at 17 km (FL550) is 4.6 $\pm$ 0.2 GV. The minimum and maximum cutoffs at this altitude are 4.3 GV and 5.2 GV, respectively. The average cutoff at 20 km (FL650) is 4.5 $\pm$ 0.2 GV. The minimum and maximum cutoff at this altitude are 4.2 GV and 4.8 GV, respectively. The cutoffs were also calculated from the NAIRAS model, as described for the RaD-X balloon flight in section 4.1.

4.3. CSBF Aircraft

All altitudes referenced in this section are geodetic altitudes, which are defined as the distances above the local ground surface.

CSBF's Cessna Conquest II chase/termination aircraft took off from Fort Sumner on 27 September 2015 at approximately 16:30 UTC. The aircraft reached a cruise altitude of 8 km at 16:37 UTC and remained at this altitude for 4 h. After takeoff, the aircraft flew northeast of Fort Sumner and followed a clockwise trajectory before returning to the airport at Fort Sumner. The flight pattern took the aircraft near Amarillo, Lubbock, and El Paso, Texas. The aircraft also flew near Roswell, Las Cruces, and Albuquerque, New Mexico.

The variation in geomagnetic cutoff rigidity was largest for the CSBF aircraft since this flight covered a wider range of latitudes compared to either the RaD-X balloon or ER-2 aircraft flights. The average cutoff is 3.6 ± 0.3 GV. The minimum and maximum cutoffs are 3.3 GV and 4.2 GV, respectively. Like the previous two flights, the cutoffs were calculated from the NAIRAS model.

4.4. Lufthansa Aircraft

All altitudes referenced in this section are barometric altitudes.

The Lufthansa commercial flights that participated in the DLR dosimetric measurement campaign were flights from Germany to Japan and back [*Meier et al.*, 2016]. This particular commercial flight route was chosen because the average geomagnetic cutoff rigidity is close to the average cutoff for the RaD-X balloon flight. The dosimetric measurements on the Frankfurt, Germany to Nagoya, Japan flight were averaged over a 60 min period between 19:42 and 20:41 UTC on 12 September 2015, for a range of geomagnetic cutoff rigidities between 3.2 GV and 4.9 GV. The cruise altitude over this averaging period was 11.3 km (FL370). The return flight from Nagoya to Frankfurt occurred on 15 September 2015. The dosimetric measurements on this flight were averaged over a 63 min period from 03:48 to 04:50 UTC for same range of cutoffs. The cruise altitude for this averaging period is 10.4 km (FL340). The average geomagnetic cutoff rigidity for both flights is 4.1 GV, which was calculated using the PLANETOCOSMICS tool [*Meier et al.*, 2016].

5. Results and Discussion

The dosimetric quantities measured by the TEPC, Liulin, and TID instruments during the RaD-X balloon flight are shown in Figures 6 and 7. Each data point in these figures represents a 1 min average. Measurements from the RaySure are analyzed in a separate paper in this special issue [*Hands et al.*, 2016].

Figure 6 shows the absorbed dose rates in tissue measured by the TEPC; absorbed dose rates in silicon are measured by the Liulin and TID. The passage of the balloon through the Pfotzer maximum during the ascent can be discerned by a peak region in the TEPC, Liulin, and TID absorbed dose rates about an hour after launch. The Pfotzer maximum region was detected by the TEPC around 17:59 UTC. The peak in the TEPC 1 min absorbed dose rate data was 3.5 μGy/h, which occurred at 18:05 UTC, as the balloon passed through the Pfotzer maximum. The peak region of the absorbed dose rates measured by the Liulin occurs earlier in time or at lower altitudes than the TEPC. This is due to relatively larger statistical fluctuations in the Liulin absorbed dose rates, which bias the apparent location of the Pfotzer maximum and the peak dose rate derived during the ascent phase of the balloon. The statistical fluctuations in the TID absorbed dose rates are the largest of RaD-X instruments, for reasons discussed below. When the high-frequency statistical fluctuations in the Liulin and TID absorbed dose rates are filtered out, the subsequent Pfotzer maximum altitude and peak absorbed dose rate derived from these instruments are in much better agreement with the TEPC (see discussion of Figures 8–10).

The statistical variations in the Liulin and TID absorbed dose rates in Figure 6 are larger than observed in the laboratory exposures prior to launch [*Straume et al.*, 2016]. The statistical fluctuations in the TID flight data are the largest of all the RaD-X instruments. Analysis of the engineering data taken during the prelaunch Thermal Altitude Test (TAT) of the integrated balloon payload revealed a component of voltage noise superimposed on the TID power supply line by a DC-DC converter, which provided the voltage interface between the RaySure and the avionics power distribution board. This noise source was taken as an accepted risk since the 15 Hz sampling of the TID output pins would enable a significant reduction in statistical uncertainty in computing the flight-averaged absorbed dose rates given in Table 4. A postflight analysis of the engineering data confirmed that voltage noise was induced on the TID power line by the DC-DC converter. The postflight analysis also showed discernible noise fluctuations in the Liulin power supply line, which may in part explain the relatively larger statistical fluctuations in the flight data compared to the laboratory exposures.

Figure 7 shows the radiobiological dose rates measured by the TEPC: dose equivalent and H*(10). These are the dosimetric quantities related to health risk and used in radiation protection applications [*ICRU*, 2010; *ICRP*, 2007]. The magnitude of these quantities in the atmospheric radiation environment displays significantly greater point-to-point variation compared to absorbed dose rates since stochastic, single high-LET events greatly influence the radiobiological dose quantities through the enhanced weighting of high-LET events by the quality factor $Q(L)$ [*ICRU*, 2010]. The temporal variations in the radiobiological dose rates for the balloon

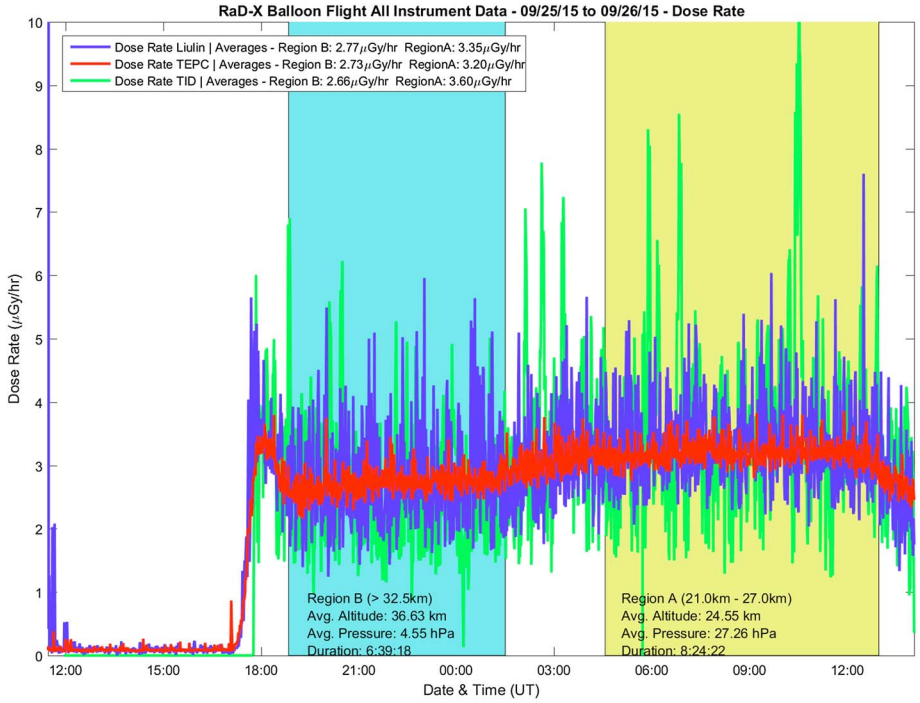

Figure 6. Absorbed dose rate measurements during RaD-X balloon flight. TEPC measured absorbed dose rate in tissue (red line); Liulin (blue line) and TID (green line) measured absorbed dose rates in silicon.

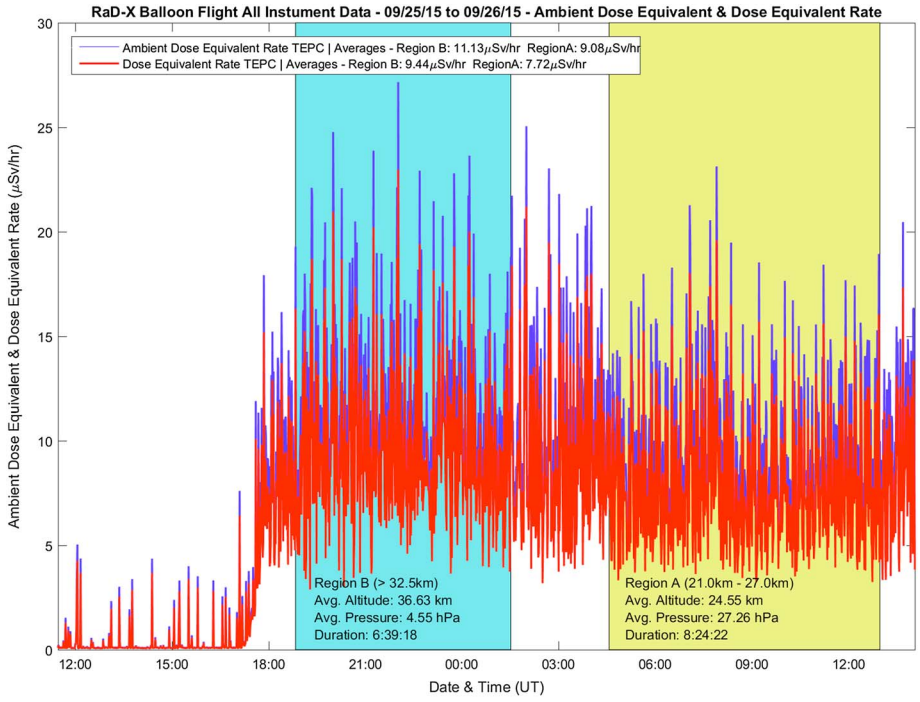

Figure 7. The radiobiological dosimetric quantities measured by the TEPC during the RaD-X balloon flight: H*(10) rate (blue line) and dose equivalent rate (red line).

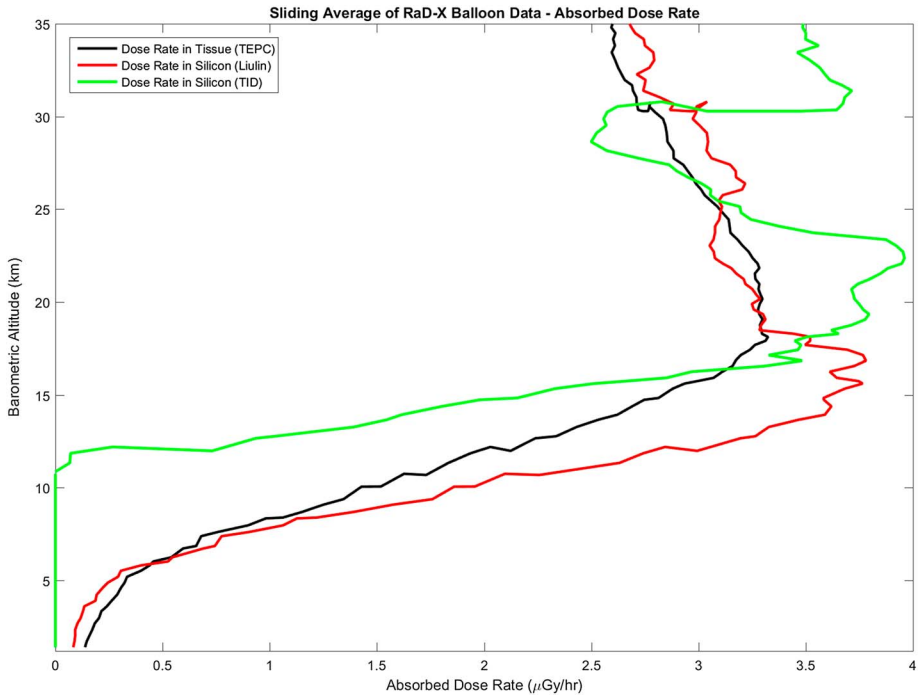

Figure 8. Altitude profiles of absorbed dose rates measured in tissue (TEPC) and in silicon (Liulin and TID) during the ascent phase of the RaD-X balloon flight using a ±10 min window average: TEPC (black line), Liulin (red line), and TID (green line).

flight are similar to corresponding measurements taken on commercial aircraft flights [*Mertens et al.*, 2013; *Meier et al.*, 2009]

High-resolution altitude profiles of the dosimetric quantities are difficult to extract from the flight measurements since the balloon ascends fairly rapidly (~5.2 m/s) through the atmosphere in a low-intensity radiation environment. Therefore, as an added consistency check, two techniques were employed to derive altitude profiles of the average dose rate quantities. The first approach is to compute the dosimetric quantities as a function of altitude during the ascent of the balloon, from just prior to launch to the highest altitude attained in Region B, using a ±10 min sliding window average. Figure 8 shows the altitude profiles of absorbed dose rates obtained from the TEPC, Liulin, and TID data using the sliding window average. This technique works fairly well for the TEPC data since the derived absorbed dose rate altitude profile is consistent with expected results [*Dachev*, 2013; *Wilson et al.*, 2003]. One of the advantages of the TEPC instrument is its large detector volume, which yields relatively lower statistical uncertainty as compared to the other RaD-X instruments. Based on the TEPC absorbed dose rate data shown in Figures 6 and 8 (black line), the balloon passed through the Pfotzer maximum region from about 17:59 UTC (18.2 km) to 18:17 UTC (22.3 km), corresponding to an average altitude for the Pfotzer maximum of 20.2 km.

The statistical fluctuations in the Liulin and TID absorbed dose rate data are relatively large compared to the TEPC, as seen in Figure 6. The larger statistical variations in the two silicon detectors are conjectured to originate from two sources. First, The TEPC detector volume is much larger than the Liulin and TID. The TID has the smallest detector volume. Thus, the TEPC will have the lowest statistical uncertainty in a given time interval compared to the Liulin or TID. Correspondingly, the TID will have the largest statistical uncertainty. Second, as previously discussed, the DC-DC converter induced an additional noise component into the TID flight data, and possibly introduced a noise component into the Liulin flight data as well.

The statistical fluctuations in both the Liulin and TID data are large enough to bias the shape and magnitude of the altitude profile of the average absorbed dose rates obtained using the sliding window average technique. This is clearly noticeable in the Liulin and TID altitude profiles of absorbed dose rates shown in Figure 8. However, if the high-frequency fluctuations in the Liulin and TID absorbed dose rates are filtered out, the subsequent altitude profile is in better agreement with the TEPC data and with the expected altitude

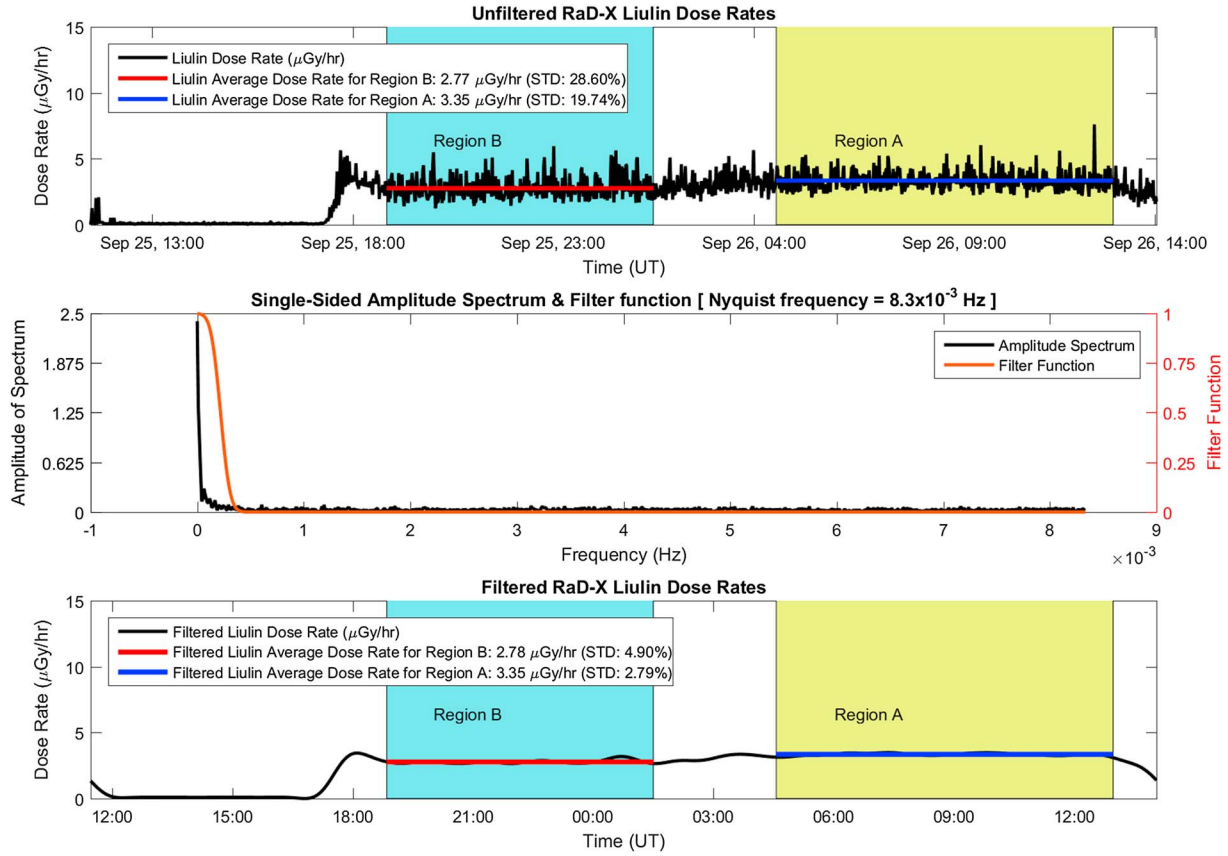

Figure 9. (top) The time series of absorbed dose rates in silicon measured by the Liulin during the RaD-X balloon flight, which corresponds to the Liulin data shown in Figure 6. (middle) The Fourier transform of the Liulin dose rate time series (black line) and a low-pass filter (red line) used to filter out the high-frequency components of the dose rate time series spectrum. (bottom) The filtered Liulin absorbed dose rate time series: inverse Fourier transform of the product of the quantities are shown in Figure 9 (middle).

structure of absorbed dose rates in silicon [*Dachev*, 2013], as demonstrated by the results shown in Figure 10. This filtering technique is the second approach utilized in extracting altitude profiles of the dosimetric quantities from the balloon flight measurements.

The process employed to remove the statistical fluctuations in the Liulin and TID absorbed dose rate data was the application of a low-band-pass filter to the Fourier transform of the corresponding absorbed dose rate time series in Figure 6. The low-band-pass filter effectively eliminated the high-frequency fluctuations in the absorbed dose rate time series spectrum. Figure 9 illustrates the main steps of this technique for the Liulin flight data. Figure 9 (top) shows the absorbed dose rate time series for the balloon flight (same as Liulin time series data shown in Figure 6). Figure 9 (middle) shows the time series spectrum and the filter function. Figure 9 (bottom) shows the inverse Fourier transform of the product of the filter function and the time series spectrum. This same filtering technique was applied to the TID absorbed dose rate data as well. The subsequent altitude profiles of the Liulin and TID absorbed dose rates obtained from the Fourier transform filtering method are presented in Figure 10. The reasonableness of this approach is that the filtered flight data reproduced the flight-averaged absorbed dose rates for Regions A and B reported in Tables 3 and 4, which were computed from the unfiltered 1 min absorbed dose rate data shown in Figure 6. In other words, the filtering technique did not bias the flight-averaged dosimetric quantities computed over the two science regions. Moreover, the Liulin and TID altitude profiles in Figure 10 are in much better agreement with the TEPC data and expected results.

For completeness, the Fourier transform filtering technique was also applied to the TEPC absorbed dose rate data. These results are also shown in Figure 10. Because of the TEPC's large detector volume and relatively low statistical uncertainty, the Fourier transform filtering technique only slightly altered the altitude profile with

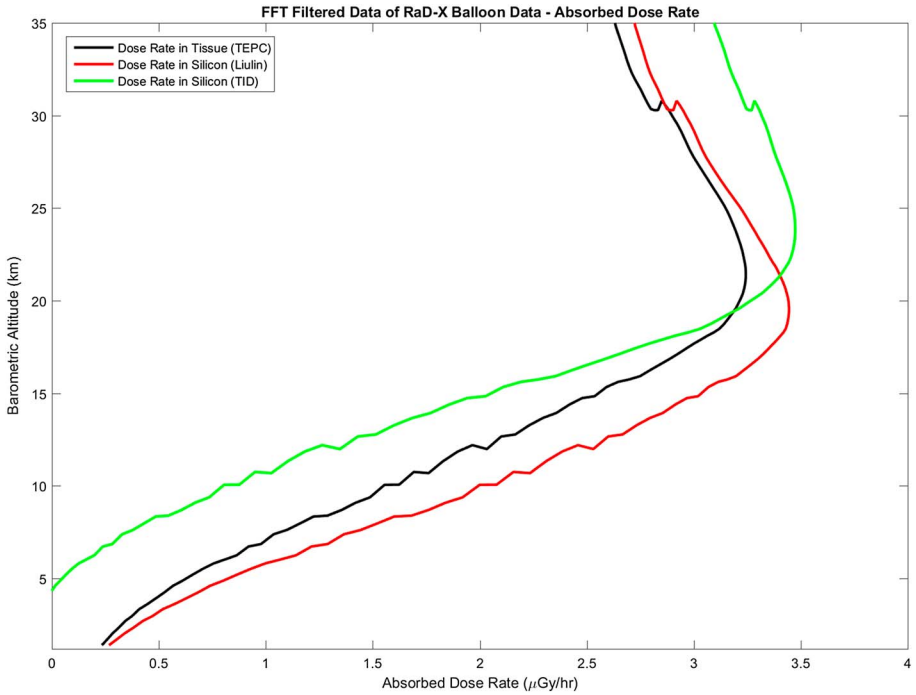

Figure 10. Altitude profiles of absorbed dose rates measured in tissue (TEPC) and in silicon (Liulin and TID) during the ascent phase of the RaD-X balloon flight using the Fourier transform filtering: TEPC (black line), Liulin (red line), and TID (green line).

respect to the sliding window average method. This was the anticipated result, adding confidence in using this filtering technique to extract altitude profiles of the dosimetric quantities from the balloon measurements.

The characteristics of the Pfotzer maximum derived from the TEPC, Liulin, and TID absorbed dose rate profiles shown in Figure 10 are the following. The peak absorbed dose rate in tissue obtained from the TEPC is 3.2 μGy/h. The altitude of the peak absorbed dose rate is 21.2 km. The peak absorbed dose rate in silicon obtained from the Liulin data is 3.4 μGy/h, which occurs at an altitude of 19.6 km. From the TID data, the peak absorbed dose rate in silicon is 3.5 μG/h, which is located at an altitude of 23.7 km. The peak absorbed dose rates derived from these three instruments are within 10% of each other. The altitude of the Pfotzer maximum obtained from the TID data is 2.5 km higher than the TEPC, while the Liulin is 1.6 km lower than the TEPC. The altitude profiles of the TEPC absorbed dose rates extracted using the sliding window average and the Fourier transform filtering technique are nearly the same. The altitude profile and the Pfotzer maximum characteristics derived from the TEPC flight data are likely the most accurate of the RaD-X instruments.

Table 3. RaD-X Campaign Flight-Averaged Dosimetric Quantities and Estimated Total Uncertainty[b]

Barometric Altitude (km)	Atmospheric Pressure (hPa)	Flight Platform	Cutoff Rigidity (GV)	Liulin Dose Rate (μGy/h)	TEPC Dose Rate (μGy/h)	TEPC Dose Equation Rate (μSv/h)	TEPC ⟨Q⟩ (Unitless)	TEPC H*(10) (μSv/h)
8.0[a]	444.9	CSBF	3.62 ± 0.32	0.94 ± 0.05	0.90 ± 0.18	2.44 ± 0.50	2.60 ± 0.75	N/A
10.4	249.0	DLR	4.10 ± 0.80	1.43 ± 0.15	N/A	N/A	N/A	4.73 ± 0.37
11.3	216.0	DLR	4.10 ± 0.80	1.77 ± 0.18	N/A	N/A	N/A	5.54 ± 0.45
17.0	92.0	ER-2	4.60 ± 0.21	N/A	4.75 ± 0.95	9.20 ± 1.85	1.99 ± 0.56	N/A
20.0	85.6	ER-2	4.51 ± 0.15	N/A	5.40 ± 1.08	11.08 ± 2.25	2.11 ± 0.60	N/A
24.6	27.3	RaD-X	3.81 ± 0.09	3.34 ± 1.04	3.20 ± 0.48	7.70 ± 1.16	2.37 ± 0.50	9.05 ± 1.37
36.6	4.5	RaD-X	3.52 ± 0.08	2.77 ± 0.86	2.73 ± 0.41	9.40 ± 1.42	3.40 ± 0.72	11.09 ± 1.67

[a]Unit is geodetic altitude.
[b]Total uncertainty is root-mean-square of systematic and statistical uncertainties.

Table 4. RaD-X Balloon Flight-Averaged Dosimetric Quantities Corrected for Payload Structure Effects

Barometric Altitude (km)	TID Dose Rate (μGy/h)	Liulin Dose Rate (μGy/h)	TEPC Dose Rate (μGy/h)	TEPC Dose Equation Rate (μSv/h)	TEPC H*(10) (μSv/h)
24.6	3.52 ± 0.70	3.42 ± 1.04	3.05 ± 0.48	7.76 ± 1.16	9.13 ± 1.37
36.6	2.55 ± 0.51	2.82 ± 0.86	2.58 ± 0.41	9.38 ± 1.42	11.06 ± 1.67

Figure 11 shows the altitude profile of the TEPC dose equivalent rate, which was derived using the two techniques discussed above. The black line in Figure 11 shows the dose equivalent rate computed from TEPC measurements during the ascent phase of the balloon flight using the ±10 min sliding window average. The green line in Figure 11 shows the altitude profile using the Fourier transform filtering technique on the flight time series of dose equivalent rate data shown in Figure 7.

The most important characteristic of the TEPC dose equivalent rate profile in Figure 11 is the absence of a distinct Pfotzer maximum. The dose equivalent rate increases with altitude until it reaches a plateau at the conventional Pfotzer maximum, as seen in the TEPC absorbed dose rate profile in Figure 10. The absence of a distinct Pfotzer maximum in dose equivalent rate was not observed in previous balloon flights where the onboard dosimeters were largely insensitive to high-LET events [*Advisory Committee for Radiation Biology Aspects of the SST (ACRBASST)*, 1975; *Foelsche et al.*, 1974; *Wissmann et al.*, 2013]. A plateau in the dose equivalent rate occurs at about 21 km in the profile computed using the sliding window average. The statistical significance of this computed average dose equivalent rate profile is illustrated in Figure 12, where the horizontal error bars are the standard deviations of the mean shown at various altitudes in the ascent data. It is clear that the absence of a distinct Pfotzer maximum is statistically significant, which was also seen in the RaySure dose equivalent rate profile derived from the RaD-X balloon flight data [*Hands et al.*, 2016].

The dose equivalent rate altitude profile derived from the Fourier transform filtering technique also displays an absence of a distinct Pfotzer maximum. This result is also shown in Figure 11. However, in this case, the plateau occurs from about 21 km to 27 km, with a slight increasing trend in dose equivalent rate for altitudes above 32 km. It is difficult to determine whether the increase in dose equivalent rate for altitudes greater than 32 km is because the Fourier transform filtering technique extracted from the TEPC flight measurements is a

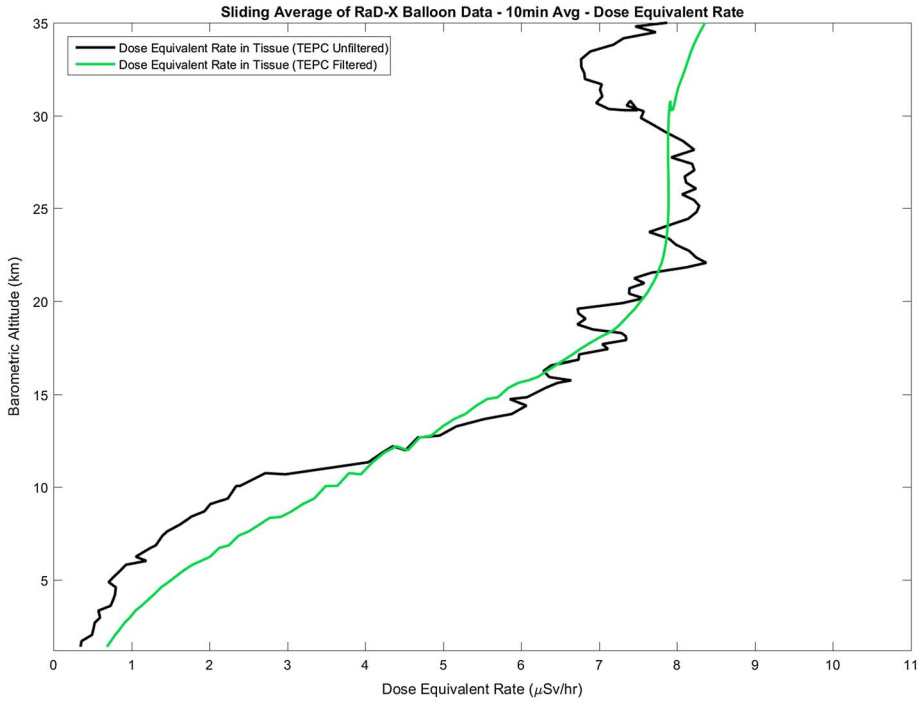

Figure 11. Altitude profile of dose equivalent rate measured by the TEPC during the ascent phase of the RaD-X balloon flight: ±10 min window average (black line) and after noise filtering the flight time series data.

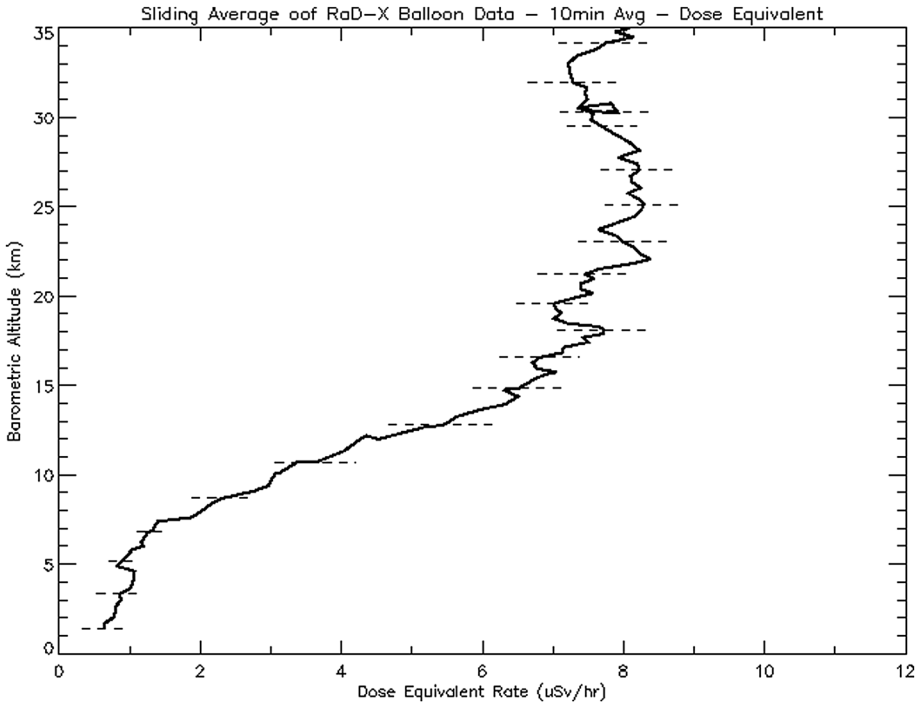

Figure 12. Dose equivalent rate measured by the TEPC during the ascent phase of the RaD-X balloon flight. The dose equivalent rate profile was computed from the 1 min TEPC data using the ±10 min sliding window average. The horizontal error bars are the standard deviation of the mean at various data points.

true secular trend in the dose equivalent rate profile, or whether the technique introduced a bias in the altitude structure of the computed average dose equivalent rate. Nevertheless, it is noteworthy to mention that the increase in the dose equivalent rate above 32 km is consistent with the influence of heavy-ion cosmic ray primaries [*Norman et al.*, 2016]. Within the conceptual framework of state-of-the-art cosmic radiation transport models, the differences between the vertical shape of the absorbed dose rate and dose equivalent rate in the region of the conventional Pfotzer maximum is the result of a complex mixture of high-LET and low-LET radiations, originating from both cosmic ray primaries and secondaries.

The TEPC and Liulin spectral dose measurements provide useful observational constraints for characterizing the dosimetric properties of cosmic ray primaries. Both instruments measure spectral dose from high-LET and low-LET radiations. As shown below, the differences between the high-LET radiation component in Regions A and B are statistically significant in both the TEPC and Liulin measurements. Moreover, the Liulin dosimetric quantities are dominated by charged particle and electromagnetic contributions, while the TEPC is able to detect neutron contributions to the dose quantities. Consequently, the spectral measurements of the high-LET and low-LET radiations in the two science regions, combined with the different particle responses of the TEPC and Liulin instruments, can be utilized to provide a better observation-based characterization of the influence of cosmic ray primaries on the dosimetric quantities than currently exist. Furthermore, these measurements will be beneficial to improving aviation radiation models by providing useful observations for teasing out the physics of the production and transport of secondary radiation, which is the source of radiation exposure at aircraft altitudes.

The Liulin energy deposition spectrum is consistent with a greater number of high-LET events in Region B compared to Region A. Figure 13 shows the Liulin's relative spectral dose distribution versus LET. LET was approximated by dividing the energy deposited in each channel by the thickness of the silicon detector disk. The dose rates are higher in Region B compared to Region A for LET > 10 keV/μm. The difference in spectral dose between Regions A and B is quantified by averaging the relative dose in Figure 13 (top) into low-LET and high-LET spectral bands, as shown in Figure 13 (bottom). The standard deviations of the relative spectral dose per low/high-LET bands are also shown in Figure 13 (bottom). The higher relative contribution to

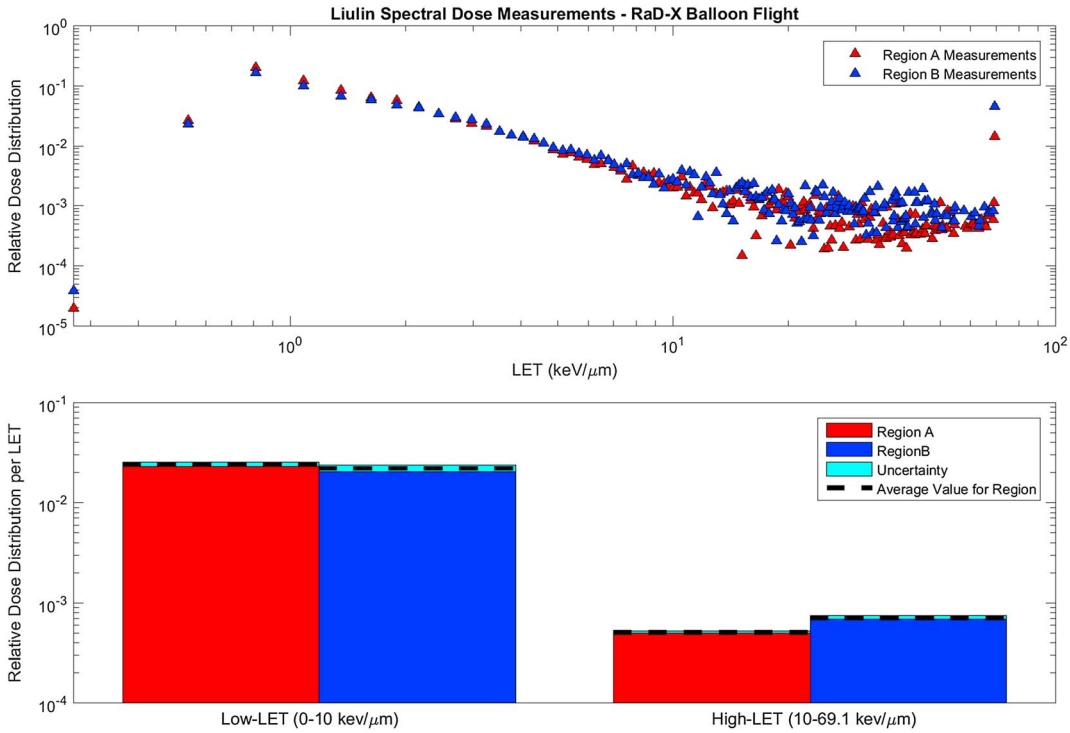

Figure 13. (top) Relative dose distribution versus LET in silicon derived from Liulin measurements averaged over Regions A and B of the RaD-X balloon flight. LET was approximated by dividing the deposited energy of the Liulin's spectral channels by the thickness of the silicon detector disk. (bottom) Average relative dose spectra of Regions A and B averaged in low-LET and high-LET bands.

absorbed dose rate from high-LET (>10 keV/μm) events in Region B compared to Region A is statistically significant. Thus, the dose distributions in these two science regions display very different energy deposition characteristics. These differences are even more conspicuous in the TEPC LET spectra.

The TEPC is able to detect significantly higher LET events compared to the other RaD-X science instruments (see Tables 1 and 2). Figure 14 shows the relative spectral dose distribution (hereafter referred to as simply dose distribution [*Chang and Kim*, 2008]) for the RaD-X balloon flight at Regions A and B. Similar to the Liulin results, the TEPC dose distributions in these two science regions display very different energy deposition

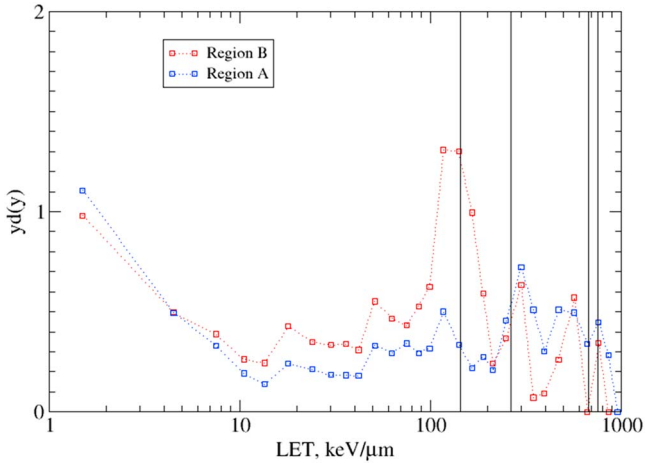

Figure 14. Lineal dose distribution (d(*y*)) derived from TEPC measurements in Regions A and B of the RaD-X balloon flight. The lineal energy is denoted *y* (keV/μm). The dose distributions were derived from the LET count spectrum integrated over the time periods spent in each region. From left to right, the vertical lines denote the proton, alpha, carbon, and nitrogen edge points, respectively. See text for details.

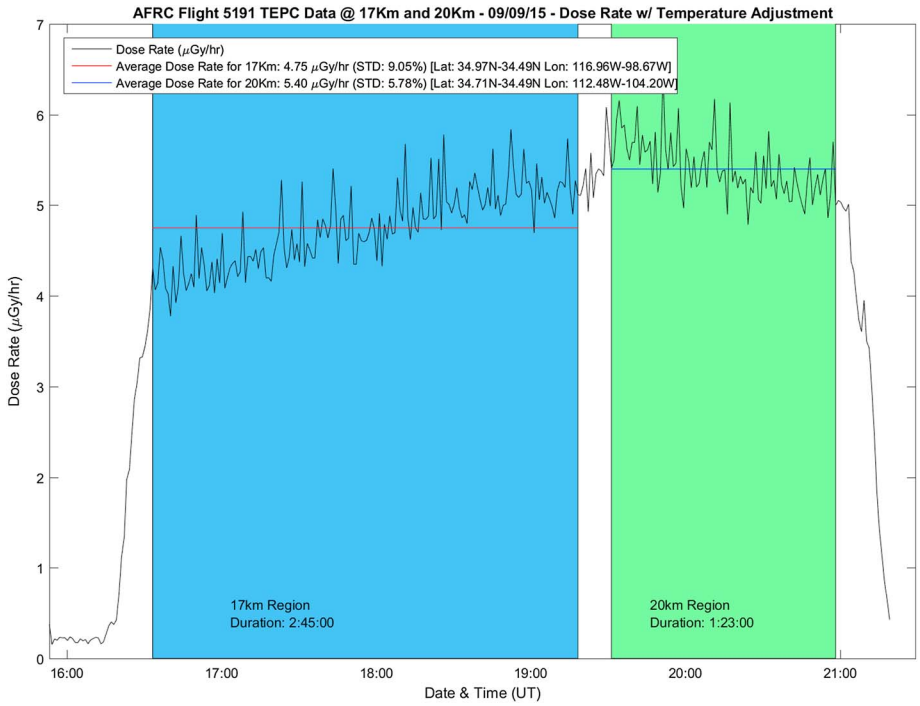

Figure 15. Absorbed dose rates measured by SolarMetric's Hawk version 2.0 TEPC during the NASA AFRC ER-2 flight. The standard deviations (STD) reported in the legend were computed from the 1 min measurements over the altitude region indicated.

characteristics. The contributions to absorbed dose for LET > 4–5 keV/μm are greater in Region B compared to Region A. The ability of the TEPC to detect higher LET events than the Liulin reveals a significant peak in the Region B dose distribution at roughly 150 keV/μm. In Region A, most of the contributions to absorbed dose come from LET <10 keV/μm. In Region B, on the other hand, a nonnegligible fraction of the total absorbed dose is coming from the peak at ~150 keV/μm.

It is interesting to note in Figure 14 that the peaks in the TEPC's dose distribution for LET >100 keV/μm are in close alignment with the edge points for the main target fragments of the A-150 tissue equivalent plastic [*Walker*, 1995]. A simple calculation using the SRIM range-energy database [*Ziegler et al.*, 2008] shows that the proton edge is at ~144 keV/μm. The alpha edge from the (n, α) reaction is located at ~263 keV/μm. The carbon and nitrogen edge points are at ~677 keV/μm and 752 keV/μm, respectively. Thus, the edge points from the main A-150 target fragments, along with the alpha edge, line up very closely with the peaks in the dose distribution shown in Figure 14. Within this conceptual framework, there is a significantly larger contribution to dose in Region B from recoil protons. *Norman et al.* [2016] concluded that scalar dosimetric quantities are insufficient to fully resolve the discrepancies between the RaD-X balloon flight measurements and model predictions. Consequently, spectral measurements are also needed to assess and ultimately improve cosmic radiation transport models. To our knowledge, stratospheric spectral dosimetric measurements for LET > 100 keV/μm have not been previously published. As a result, the TEPC dose distribution measurements at the RaD-X science regions will provide an important data set for testing and validating physics-based atmospheric ionizing radiation models.

The remaining figures are examples of the dosimetric measurements taken from the supporting aircraft flights. Figure 15 shows the absorbed dose rates in tissue measured by the TEPC on the NASA AFRC ER-2 aircraft. By comparing Figure 15 with Figure 6, the absorbed dose rates measured during the ER-2 flight are larger than the corresponding measurements taken on the RaD-X balloon. This is because the two cruise altitudes of the ER-2 flight are in the vicinity of the Pfotzer maximum.

For the ER-2 flight data, the TEPC dosimetric quantities were corrected for temperature variations of the propane gas inside the detector chamber. The pressurized aluminum TEPC container was not temperature controlled during the ER-2 flight. The manufacturer's reported uncertainty is based on maintaining the

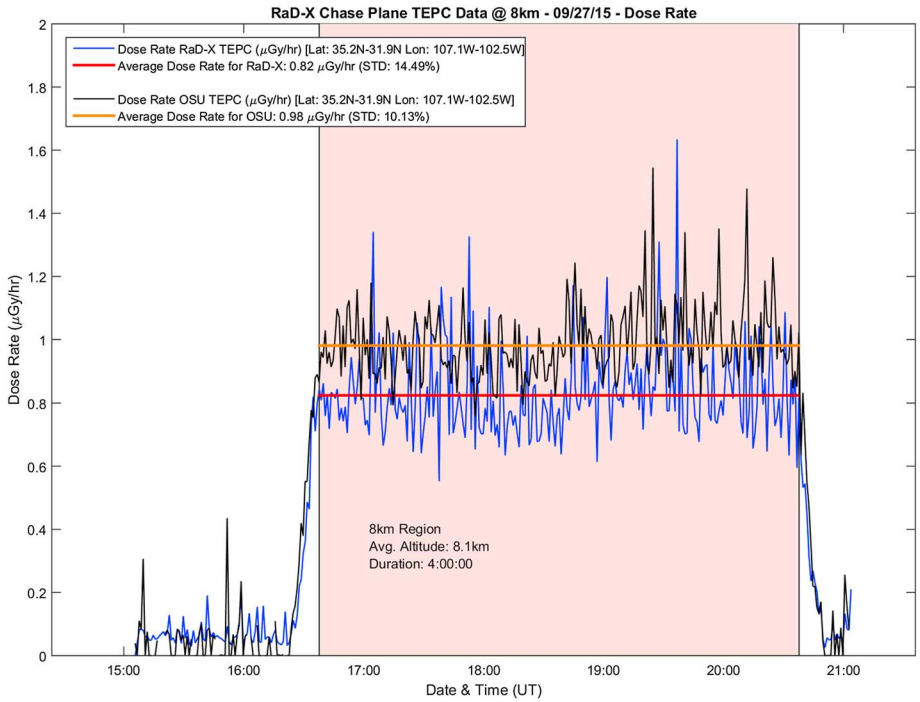

Figure 16. Measurements of absorbed dose rates in tissue taken during the CSBF aircraft flight by two onboard TEPCs: the Hawk version 3.0 RaD-X flight spare and the Hawk version 2.0 from Oklahoma State University. The standard deviations (STD) reported in the legend were computed from the 1 min measurements over the altitude indicated.

propane gas temperature between 15°C and 35°C [*Conroy*, 2011]. The temperature at the 17 km cruise altitude varied from 10°C to 35°C. The temperature at the 20 km cruise altitude remained at 9°C. The dosimetric quantities reported in Table 3 were corrected for the propane gas temperature variation using an adjustment factor of 0.5% change in dosimetric quantity per degree Celsius with reference to 25°C [*Conroy*, 2011]. Adjustments to the RaD-X balloon flight TEPC dosimetric quantities were not necessary since the pressurized aluminum container that housed the TEPC was temperature controlled. The temperature of the propane gas during the RaD-X flight was maintained between 22°C and 27°C.

The absorbed dose rates measured during the CSBF aircraft flight are shown in Figures 16 and 17. Absorbed dose rates in tissue were taken by the RaD-X Hawk version 3.0 TEPC flight spare and a Hawk version 2.0 TEPC. The flight-averaged dose rates measured by the two independent TEPCs shown in Figure 16 differed by just under 20%, which is within the range of measurement uncertainty reported for the GCR radiation environment at commercial aircraft altitudes [*Lindborg et al.*, 2004]. Figure 17 shows the Liulin absorbed dose rates in silicon measured during the CSBF flight.

A summary of the TEPC and Liulin flight-averaged dosimetric quantities for the RaD-X campaign is given in Table 3. The average quality factor, $\langle Q \rangle$, is also listed for the TEPC measurements. The uncertainties reported for the geomagnetic cutoff rigidity are the standard deviations of the NAIRAS model predictions computed over each flight path. The uncertainties reported for the dosimetric quantities are the root-sum-square of the systematic and statistical uncertainties. The statistical uncertainties were computed at each flight level listed in Table 3 as the standard deviation of the mean, which was less than 2% for the absorbed dose rate data and less than 5% for the radiobiological dose rate quantities. The systematic uncertainties were treated conservatively, taking the largest estimate if multiple assessments were available. The systematic uncertainty for the RaD-X TEPC flight data was taken to be 16%, based on laboratory calibration using reference high-LET and low-LET radiation sources [*Straume et al.*, 2016]. The 20% difference between the two TEPCs on the CSBF flight was taken as the systematic uncertainty for both the CSBF and ER-2 TEPC flight data. The systematic uncertainty for the CSBF Liulin flight data was taken to be 5%, based on comparisons to TEPC absorbed dose rate data on commercial aircraft flights [*Dachev et al.*, 2015]. The RaD-X Liulin absorbed dose rate

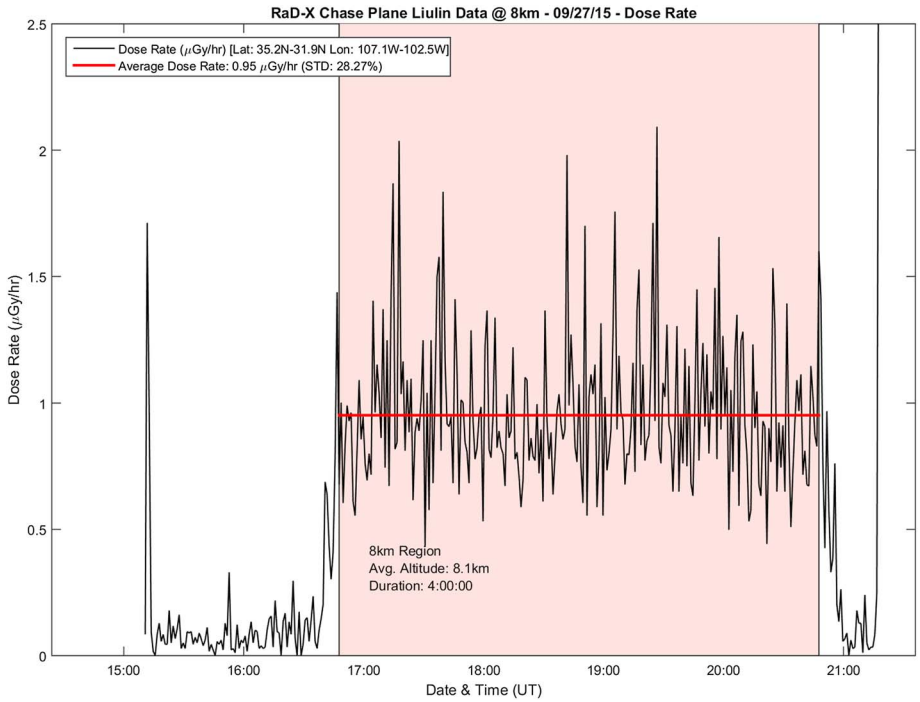

Figure 17. Measurements of absorbed dose rates in silicon taken during the CSBF aircraft flight by the Liulin-4 provided by Oklahoma State University. The standard deviation (STD) reported in the legend was computed from the 1 min measurements over the altitude indicated.

measurements differed from the laboratory reference low-LET radiation source by 31%, which was taken as the systematic uncertainty for the balloon flight data. The systematic uncertainty for the TID flight data was taken to be 20% [*Mazur et al.*, 2011].

As discussed earlier in this section, the 15 Hz sampling of the TID output pins enabled the statistical uncertainty of the derived absorbed dose rates to be significantly reduced, despite the induced noise by the DC-DC converter. The TID is the most susceptible of the RaD-X instruments to large statistical uncertainty in the absorbed dose rates, for several reasons. First, the atmosphere is a low-intensity ionizing radiation environment and the TID detector volume is small (the smallest of the four RaD-X instruments). Second, the fundamental dosimetric quantity obtained from the TID is accumulated dose [*Mazur et al.*, 2011], which means that absorbed dose rates are derived by computing numerical derivatives of the accumulated dose measurements [*Straume et al.*, 2016]. The 15 Hz sampling of the TID output pins was designed to reduce the statistical uncertainty in the derived absorbed dose rates by employing an interleave technique described in more detail below. The 15 Hz sampling had sufficient margin to reduce the statistical uncertainty below 1% in computing the flight-averaged absorbed dose rates in Regions A and B, even with the additional noise induced by the DC-DC converter.

The processing of the TID absorbed dose rates is described as follows. The voltage output pins of the TID were oversampled at 15 Hz by the onboard data acquisition system. The science processing algorithm subsampled the voltages at 5 min intervals. The accumulated dose was then calculated at the 5 min intervals throughout the duration of the flight data using a voltage-to-dose conversion factor [*Lindstrom et al.*, 2011; *Mazur et al.*, 2011; *Straume et al.*, 2016]. The absorbed dose rates were computed at the 5 min time intervals by numerical differentiation of the accumulated dose data. The starting measurement in the processing of the output voltages, from which the time series of flight accumulated dose were computed at the 5 min intervals, was advanced by one sample point (1/15 s). At this new starting point, the output voltages were again subsampled at 5 min increments. Hence, the accumulated doses were calculated at the new time series of 5 min intervals, from which the absorbed dose rates were determined as before. This sequence was repeated until all 15 Hz data were utilized. All the absorbed dose rate time series at the 5 min increments were combined (i.e., interleaved) into a single, contiguous time series at the 1/15 s grid spacing. These absorbed dose rates

were subsequently averaged in 1 min intervals corresponding to the time intervals of the TEPC and Liulin data. Thus, 900 absorbed dose rate data points were averaged in each 1 min interval. The result of this interleave processing technique is the TID flight data shown in Figure 6. The mean absorbed dose rates in Regions A and B are 3.60 μGy/h and 2.66 μGy/h, respectively. The standard deviations of the mean in the two science regions are less than 1%. Outliers were rejected in computing the mean and standard deviation using Chauvenet's criterion [*Taylor*, 1982].

The flight-averaged dosimetric quantities for the RaD-X balloon flight were also corrected for the influence of the payload structure. The payload structure, including, for example, the sealed aluminum container enclosing the TEPC, are potential sources of secondary radiation as the ambient radiation field interacts with the intervening material between the atmosphere and the science instruments. Payload structure correction factors were derived for the TEPC, Liulin, and TID instruments using Geant-4 Monte Carlo radiation transport simulations, combined with a detailed Computer-Aided Design (CAD) model of the RaD-X science payload [*Gronoff et al.*, 2016]. The results of applying these correction factors to the flight-averaged dosimetric quantities are given in Table 4. The structure-corrected quantities in Table 4 represent the dosimetric quantities measured by the instruments in the absence of the payload structure. The effect of the payload structure on the measured dosimetric quantities is less than 7%, which is much less than the systematic uncertainty of the instrument measurements themselves. The simulations also indicated that the TID and Liulin were largely insensitive to neutrons in the atmospheric radiation environment. This result was corroborated by the instrument exposures to the laboratory radiation sources as well [*Straume et al.*, 2016].

The ratio of the average absorbed dose rate measured by the TEPC to the average absorbed dose rate measured by the Liulin is 0.90 for the RaD-X balloon flight. This value is much lower than expected. A theoretical calculation of the ratio of the absorbed dose rate in tissue to silicon, over energies relevant to cosmic radiation exposure, is reported to be 1.33 ± 0.07 [*Schwadron et al.*, 2012], which is consistent with the value of 1.40 ± 0.2 determined from Hawk version 2.0 TEPC and RaySure measurements at commercial aircraft altitudes [*Hands and Dyer*, 2009]. However, if the RaD-X balloon flight-averaged TEPC and Liulin measurements are adjusted based on their comparisons to ground-based reference radiation sources, the ratio of absorbed dose rate in tissue to silicon aligns with the expected result. The ground tests of the RaD-X science instruments showed that the TEPC underpredicted the absorbed dose rate of a reference low-LET radiation source by 16%, while the Liulin overpredicted the absorbed dose rate from the same source by 31% [*Straume et al.*, 2016]. Taking into account the underprediction of the TEPC and the overprediction of the Liulin, the adjusted average TEPC/Liulin absorbed dose rate ratio for the RaD-X balloon flight is 1.40 (0.90×1.56), which is consistent with the theoretical calculation and the measurement result derived from aircraft radiation measurements.

Furthermore, the ratio of the average absorbed dose rate in tissue to silicon derived from the RaD-X TEPC and TID flight data is consistent with the ratio computed from the RaD-X TEPC and Liulin data described above. The TEPC to TID absorbed rate ratio is 0.94. Adjusting this ratio based on the laboratory exposures produces a value consistent with 1.40 ± 0.2, which was based on aircraft radiation measurements. The TID overestimated the absorbed dose rate of the low-LET reference radiation source by 7% [*Straume et al.*, 2016]. Combining this with the 16% underprediction of the TEPC with respect to the reference low-LET radiation source, the adjusted average TEPC/TID absorbed dose rate ratio for the RaD-X balloon flight is equal to 1.20 (0.94×1.27).

The above derivation of the adjusted ratio of the absorbed dose rate in tissue to silicon using the RaD-X TEPC, Liulin, and TID measurements should be viewed with caution. First, the adjustment factors were based on instrument responses to a laboratory low-LET radiation source. However, the RaD-X balloon flight science regions are characterized by a mixed-field radiation environment, including both low-LET and high-LET radiations. Second, the ratio of the average dose rate between the TEPC and the RaySure is 1.05 for the RaD-X balloon flight [*Hands et al.*, 2016]. However, adjusting this ratio based on the laboratory exposures is not warranted in this case since both the TEPC and RaySure instruments had basically the same response to the ground-based reference low-LET radiation source [*Straume et al.*, 2016]. As noted by *Hands et al.* [2016], additional laboratory and in-flight measurements are required to provide a more rigorous observation-based characterization of the scale factor in converting between absorbed dose in tissue and silicon. Alternative data analysis methods should also be employed since the application of a single-scale factor between absorbed dose in tissue and silicon may break down [*Benton et al.*, 2010].

With respect to direct comparisons of the RaD-X flight-averaged absorbed dose rates, the TEPC, Liulin, and TID results reported in Tables 3 and 4 are in excellent agreement. The Liulin differs by no more than 12% with respect to the TEPC. The TID agrees with the Liulin and TEPC to within 5% and 14%, respectively. These differences are much less than the estimated uncertainties of the measurements.

6. Summary and Conclusions

The RaD-X flight campaign provided dosimetric measurements at seven altitudes. The altitude coverage of the flight measurements extends from the lower end of commercial aircraft flight levels (8 km) to well above the Pfotzer maximum (>32 km). The flight measurements were taken at nearly the same cutoff rigidity, enabling the statistical uncertainty in the dosimetric quantities to be reduced below 5%. Moreover, the cutoff rigidity of the flight measurements corresponds to a value where the uncertainty in aviation models are 50% or greater [*Bottollier-Depois et al.*, 2012]. The conservatively estimated total uncertainty of the flight-averaged dosimetric quantities is less than the ICRU/ICRP criterion of 30% for dose assessments [*ICRU*, 2010]. Thus, the high-quality flight-averaged dosimetric quantities provide a unique data set for improving the understanding of cosmic radiation transport in the atmosphere and human exposure in the aircraft radiation environment, which is the first goal of the RaD-X mission.

The RaD-X balloon flight from Fort Sumner, NM, collected over 18 h of dosimetric measurements above the Pfotzer maximum at two primary science regions: Region A, defined as barometric altitudes between 21 and 27 km, and Region B, defined as barometric altitudes greater than 32 km. These two altitude regions, which are above the peak in secondary particle production, enable the dosimetric contributions from cosmic ray primaries to be characterized, which are the ultimate source of radiation exposure at aviation altitudes. Model simulations, based on the deterministic HZETRN transport code, indicate that the contributions from heavy-ion cosmic ray primaries are discernible in the dosimetric measurements in Region B, while protons comprise the dominant contribution from cosmic ray primaries in Region A [*Norman et al.*, 2016].

The RaD-X balloon payload consists of four science instruments: TEPC microdosimeter, Liulin dosimeter-spectrometer, Teledyne TID detector, and the RaySure detector. The agreement between the TEPC, Liulin, and TID measurements of absorbed dose rates are within 15%, which is less than the estimated total uncertainty of the measured dosimetric quantities. The spectral dose distribution measurements provided by the TEPC and Liulin instruments demonstrate very different, statistically significant, energy deposition characteristics between Regions A and B. To our knowledge, the TEPC spectral dose distribution measurements, which extend to LET > 100 keV/μm, and the Liulin spectral dose measurements, have not been previously published at these altitudes. Consequently, the RaD-X balloon flight TEPC and Liulin spectral measurements provide an important data set for assessing and validating atmospheric cosmic radiation transport models, since scalar (integrated) dosimetric quantities alone are insufficient to resolve current discrepancies between models and measurements [*Norman et al.*, 2016].

The contemporaneous aircraft flights supplemented the RaD-X measurements and enabled altitude profiles of the dosimetric quantities to be constructed, providing an overall context of the atmospheric radiation environment coincident with the RaD-X flight, and supplying additional observational constraints for assessing aviation radiation models. The NASA AFRC ER-2 aircraft flight provided dosimetric measurements from a TEPC at barometric altitudes of 20 km and 17 km. These altitudes correspond, respectively, to near the Pfotzer maximum where the peak in secondary particle production occurs, and on the bottom side of the Pfotzer maximum where attenuation processes dominate over particle production. The Lufthansa flights provided TEPC and Liulin dosimetric measurements at typical commercial aircraft cruise altitudes. The CSBF aircraft was equipped with two independent TEPC units and a Liulin instrument. The CSBF aircraft maintained a cruising altitude of 8 km (geodetic), which provided dosimetric measurements representative of the low-altitude end of commercial aircraft flights. All flights occurred during solar and geomagnetically quiet conditions.

The TID and RaySure detectors are candidate technologies for application to real-time, continuous monitoring of the aircraft radiation environment. Characterizing the performance of these silicon-based radiation detectors is the second goal of the RaD-X mission. The advantages of the RaySure are that it is a dosimeter-spectrometer with sensitivity to high-LET events and a data processing algorithm that enables the conversion of spectral dose in silicon to dose equivalent. Overall, the RaySure agreed quite well with the TEPC, but some qualitative differences were identified that require further investigation. The details of the RaySure

measurements are presented in a separate paper in this special issue [*Hands et al.*, 2016]. The disadvantage of the RaySure is that the manufacturing production of the detector is not yet made to order.

An assessment of the application of the TID to aircraft radiation monitoring is the following. The manufacturing production of the TID, contrary to the RaySure, is made to order through Teledyne Microelectronic Technologies (http://www.teledynemicro.com/product/radiation-dosimeter). In addition, the agreement was excellent between the TID and Liulin absorbed dose rate measurements on the RaD-X balloon flight. However, the TID has several disadvantages in estimating human exposure in the aircraft radiation environment. First, many aircraft flights with both the TID and a TEPC are required to develop a calibration curve to fit the TID absorbed dose rate measurements to $H^*(10)$ [e.g., *Wissmann et al.*, 2013]. The in-flight calibration analysis should incorporate flight measurements over a solar cycle and the full range of geomagnetic cutoff rigidities and atmospheric depths relevant to commercial aircraft flights. Second, precision dose rates in the low-intensity aircraft radiation environment are limited by the large granularity of the accumulated dose measurements (i.e., accumulated dose is measured in steps of 0.14 μGy [*Lindstrom et al.*, 2011; *Mazur et al.*, 2011]) and by the necessity of deriving dose rates by numerical differentiation of the accumulated dose. On the other hand, the interleave technique utilized in analyzing the RaD-X TID flight data partially mitigates the difficulty in deriving precision dose rates in the atmospheric radiation environment and should be further explored for application to real-time radiation monitoring.

The absence of a distinct Pfotzer maximum in the dose equivalent rate was observed by the TEPC on the RaD-X balloon flight. The measured dose equivalent continues to increase with altitude, with a plateau region near the Pfotzer maximum altitude observed in the absorbed dose rate. A similar observation was made by the RaySure measurements on the RaD-X balloon flight [*Hands et al.*, 2016]. However, a peak in the dose equivalent rate was observed in previous stratospheric balloon flights [e.g., *ACRBASST*, 1975], and predicted by aviation radiation models that did not include heavy-ion cosmic ray primaries in the transport physics [e.g., *Ferrari et al.*, 1999]. Thus, the presence of a distinct peak in the dose equivalent rate at the conventional Pfotzer maximum altitude is an artifact due to incomplete physics in the models and dosimeters with limited LET range. The absence of a distinct peak in the dose equivalent rate is the result of the complex atmospheric radiation environment characterized by a mixture of high-LET and low-LET radiations produced by cosmic ray primary and secondary particles. The consistency between the RaD-X TEPC measurements of the dose equivalent rate altitude profile and the prediction of current aviation models is indicative of improvements in both measurements and models [e.g., *Copeland*, 2014; *Mertens et al.*, 2013].

The RaD-X balloon flight has also identified the need for addition flight measurement, laboratory experiments, and data analysis techniques to understand the low value of the ratio of the absorbed dose rate in tissue to silicon observed at stratospheric altitudes. At minimum, an additional stratospheric balloon flight campaign should be conducted at high-latitude and low-cutoff rigidity to measure the tissue to silicon absorbed dose rate ratio in a different radiation environment.

Future work within the RaD-X science team will comprise detailed comparisons between the RaD-X flight data and the NAIRAS model predictions. The objective of these comparisons is to improve the NAIRAS model and reduce its uncertainty at geomagnetic cutoff rigidities of the order of ~4 GV or greater [*Mertens et al.*, 2013]. In addition, the interleave technique employed to analyze the RaD-X TID flight data will be further developed and tested for application to real-time monitoring of the aircraft radiation environment [*Tobiska et al.*, 2016].

Acknowledgments
The RaD-X mission was funded by the NASA Science Mission Directorate under the Hands-On Project Experience (HOPE)-4 opportunity. Civil Servant labor costs were provided by NASA Langley Research Center (LaRC), NASA Ames Research Center, and NASA Wallops Flight Facility. LaRC also contributed to facility costs, science instrument procurements (Science Directorate), and media and outreach costs. Lawrence Livermore National Laboratory provided their facility for radiation source exposure and calibration of the science instruments. Bryn Jones from SolarMetrics (United Kingdom) provided the TEPC instrument which flew on the NASA Armstrong Flight Research Center's ER-2 aircraft. Columbia Scientific Balloon Facility provided their Cessna aircraft for a dedicated flight to support the RaD-X mission. James Rosenthal from the RaD-X engineering team provided helpful information regarding the discussion of the voltage noise on the TID power supply line. The RaD-X flight data are available from the authors upon request (Christopher.J.Mertens@nasa.gov).

References

Advisory Committee for Radiation Biology Aspects of the SST (ACRBASST) (1975), Advisory committee for radiation biology aspects of the SST: Final report. Cosmic radiation exposure in supersonic and subsonic flight, *Aviat. Space Environ. Med.*, *46*(9), 1170–1185.

American Meterological Society (2007), Integrating space weather observations and forecasts into aviation operations, Washington, D. C.

Aspholm, R., M.-L. Lindbohm, H. Paakkulainen, H. Taskinen, T. Nurminen, and A. Tiitinen (1999), Spontaneous abortions among Finnish flight attendants, *J. Occup. Environ. Med.*, *41*(6), 486–491.

Benton, E. R., E. V. Benton, and A. L. Frank (2010), Conversion between different forms of LET, *Radiat. Meas.*, *45*, 957–959.

Bottollier-Depois, J. F., P. Beck, M. Latocha, V. Mares, D. Matthiä, W. Rühm, and F. Wissmann (2012), Comparison of codes assessing radiation exposure of aircraft crew due to galactic cosmic radiation, EURADOSE Rep. 2012-03, EURADOSE, Braunschweig, Germany.

Chang, S.-Y., and B.-H. Kim (2008), Understanding of the microdosimetric quantities obtained by a TEPC, *J. Nucl. Sci. Technol. Suppl.*, *5*, 213–216.

Conroy, T. (2010), *Environmental Radiation Monitor With 5" Tissue Equivalent Proportional Counter (TEPC), Hawk Version 3, Model FWAD-3, Operations and Repair Manual*, Far West Technol., Goleta, Calif.

Conroy, T. (2011), *A New Method Using Cs-137 as the Primary Calibration Source for the Hawk Instrument, Hawk3, Model FWAD, Application Note 4.0*, Far West Technol., Goleta, Calif.

Copeland, K., H. H. Sauer, F. E. Duke, and W. Friedberg (2008), Cosmic radiation exposure of aircraft occupants on simulated high-latitude flights during solar proton events from 1 January 1986 through 1 January 2008, *Adv. Space Res.*, *42*, 1008–1029.
Copeland, K. A. (2014), Cosmic ray particles fluences in the atmosphere resulting from primary cosmic ray heavy ions and their resulting effects on dose rates to aircraft occupants as calculated with MCNPX 2.7.0, PhD thesis, Dept. of Chem. and Chem. Eng., R. Mil. Coll. of Canada, Kingston, Ontario, Canada.
Dachev, T., et al. (2002), Calibration results obtained with Liulin-4 type dosimeters, *Adv. Space Res.*, *30*(4), 917–925.
Dachev, T. P. (2009), Characterization of the near Earth radiation environment by Liulin type spectrometers, *Adv. Space Res.*, *44*, 1441–1449.
Dachev, T. P. (2013), Profile of the ionizing radiation exposure between the Earth surface and free space, *J. Atmos. Sol. Terr. Phys.*, *102*, 148–156.
Dachev, T. P., et al. (2015), Overview of the Liulin type instruments for space radiation measurement and their scientific results, *Life Sci. Space Res.*, *4*, 92–114.
Dyer, C., A. Hands, F. Lei, P. Truscott, K. A. Ryden, P. Morris, I. Getley, L. Bennett, B. Bennett, and B. Lewis (2009), Advances in measuring and modeling the atmospheric radiation environment, *IEEE Trans. Nucl. Sci.*, *56*(6), 3415–3422.
Ferrari, A., M. Pelliccioni, and T. Rancati (1999), The role of the quantities used in radiobiological protection for the assessment of the exposure to cosmic radiation, *Radiat. Prot. Dosim.*, *88*(3), 199–210.
Foelsche, T., R. B. Mendell, J. W. Wilson, and R. A. Adams (1974), Measured and calculated neutron spectra and dose equivalent rates at high altitudes; revelance to SST operations and space research, NASA TN D-7715, Natl. Aeronaut. and Space Admin., Washington, D. C.
Gaisser, T. (1990), *Cosmic Rays and Particle Physics*, Cambridge Univ. Press, Cambridge, U. K.
Gopalswamy, N., R. Mewaldt, and J. Torsti (2006), Solar eruptions and energetic particles: An introduction, in *Solar Eruptions and Energetic Particles, Geophys. Monogr. Ser.*, vol. 165, edited by N. Gopalswamy, R. Mewaldt, and J. Torsti, p. 1–5, AGU, Washington, D. C.
Grajewski, B., E. A. Whelan, C. C. Lawson, M. J. Hein, M. A. Waters, J. L. Anderson, L. A. MacDonald, C. J. Mertens, C-Y. Tseng, R. T. Cassinelli II, and L. Luo (2015), Miscarriage among flight attendants, *Epidemiology*, *26*(2), 192–203.
Gronoff, G. P., C. J. Mertens, R. B. Norman, T. Straume, and T. C. Lusby (2016), Assessment of the influence of the RaD-X balloon environment on radiation detectors, *Space Weather*, doi:10.1002/2016SW001405.
Hands, A., and C. Dyer (2009), A technique for measuring dose equivalent and neutron fluxes in radiation environments using silicon diodes, *IEEE Trans. Nucl. Sci.*, *56*(6), 3442–3449.
Hands, A. D. P., K. A. Ryden, and C. J. Mertens (2016), The disappearance of the Pfotzer-Regener maximum in dose equivalent measurements in the stratosphere, *Space Weather*, *14*, doi:10.1002/2016SW001402.
International Commission on Radiobiological Protection (ICRP) (1991), *ICRP Publication 60: 1990 Recommendations of the International Commission on Radiological Protection*, vol. 21(1–3), Pergamon Press, Oxford, U. K.
International Commission on Radiological Protection (ICRP) (2007), *ICRP Publication 103: The 2007 Recommendations of the International Commission on Radiological Protection*, vol. 37(2–4), Elsevier, Oxford, U. K.
International Commission on Radiation Units (ICRU) (1983), International Commission on Radiation Units and Measurements, Microdosimetry, ICRU Rep. 36, Bethesda, Md.
International Commission on Radiation Units (ICRU) (2010), International Commission on Radiation Units and Measurements, Reference data for the validation of doses from cosmic-radiation exposure of aircraft crew, *ICRU Rep. 84*, Oxford, U. K.
Kress, B. T., C. J. Mertens, and M. Wiltberger (2010), Solar energetic particle cutoff variations during the 29–31 October 2003 geomagnetic storm, *Space Weather*, *8*, S05001, doi:10.1029/2009SW000488.
Lauria, L., T. J. Ballard, M. Caldora, C. Mazzanti, and A. Verdecchia (2006), Reproductive disorders and pregnancy outcomes among female flight attendants, *Aviat. Space Environ. Med.*, *77*(7), 533–559.
Lillhök, J., et al. (2007), A comparison of ambient dose equivalent meters and dose calulations and constant flight altitudes, *Radiat. Meas.*, *42*, 323–333.
Lindborg, L., D. T. Bartlett, P. Beck, I. McAulay, K. Schnuer, H. Straube, and F. Spurney Eds. (eds.) (2004), Cosmic radiation exposure of aircraft crew. Compilation of measured and calculated data, Final Report of the EURADOS WG 5 to the Group of Experts established under Article 31 of the European Commission Directorate-General for Energy and Transportation. Radiation Protection Issue No. 140, Luxembourg.
Lindstrom, C. D., J. D. Sullivan, B. K. Dichter, F. A. Hanser, D. Carssow, and G. E. Galica (2011), Characterization of Teledyne microdosimeters for space weather applications, *Proc. SPIE*, *8148*, 814806, doi:10.1117/12.893814.
Mazur, J. E., W. R. Crain, M. D. Looper, D. J. Mabry, J. B. Blake, A. W. Case, M. J. Golightly, J. C. Kasper, and H. E. Spence (2011), New measurements of total ionizing dose in the lunar environment, *Space Weather*, *12*, S07002, doi:10.1029/2010SW000641.
Meier, M. M., M. Hubiak, D. Matthiä, M. Wirtz, and G. Reitz (2009), Dosimetry at aviation altitudes (2006–2008), *Radiat. Prot. Dosim.*, *136*(4), 251–255.
Meier, M. M., D. Matthiä, T. Forkert, M. Wirtz, M. Scheibinger, R. Hübel, and C. J. Mertens (2016), RaD-X: Complementary measurements of dose rates at aviation altitudes, *Space Weather*, *14*, doi:10.1002/2016SW001418, in press.
Mertens, C. J. (this issue), Overview of the Radiation Dosimetry Experiment (RaD-X) flight mission, *Space Weather*.
Mertens, C. J., B. T. Kress, M. Wiltberger, S. R. Blattnig, T. S. Slaba, S. C. Solomon, and M. Engel (2010), Geomagnetic influence on aircraft radiation exposure during a solar energetic particle event in October 2003, *Space Weather*, *8*, S03006, doi:10.1029/2009SW000487.
Mertens, C. J., B. T. Kress, M. Wiltberger, W. K. Tobiska, B. Grajewski, and X. Xu (2012), Atmospheric ionizing radiation from galactic and solar cosmic rays, in *Current Topics in Ionizing Radiation Research*, edited by M. Nenoi, InTech, Rijeka, Croatia.
Mertens, C. J., M. M. Meier, S. Brown, R. B. Norman, and X. Xu (2013), NAIRAS aircraft radiation model development, dose climatology, and initial validation, *Space Weather*, *11*, 603–635, doi:10.1002/swe.20100.
National Council on Radiation Protection and Measurements (NCRP) (2009), National Council on Radiation Protection and Measurements: Ionizing radiation exposure of the population of the United States, NCRP Rep. No. 160, Natl. Counc. on Radiat. Prot. and Radiat. Meas, Bethesda, Md.
Norman, R. B., C. J. Mertens, and T. C. Slaba (2016), Evaluating GCR environment models using RaD-X flight data, *Space Weather*, doi:10.1002/2016SW001401.
Schwadron, N. A., et al. (2012), Lunar radiation environment and space weathering from the Cosmic Ray Telescope for the Effects of Radiation (CRaTER), *J. Geophys. Res.*, *17*, E00H13, doi:10.1029/2011JE003978.
Silari, M., et al. (2009), Intercomparison of radiation protection devices in a high-energy stray neutron field. Part III: Instrument response, *Radiat. Meas.*, *44*, 673–691.
Straume, T., C. J. Mertens, T. C. Lusby, B. Gersey, W. K. Tobiska, R. B. Norman, G. P. Gronoff, and A. Hands (2016), Ground-based evaluation of dosimeters for NASA high-altitude balloon flight, *Space Weather*, doi:10.1002/2016SW001406.
Taylor, J. R. (1982), *An Introduction to Error Analysis, the Study of Uncertainties in Physical Measurements*, Univ. Science Books, Mill Valley, Calif.

Tobiska, W. K., et al. (2016), Global real-time dose measurements using the Automated Radiation Measurements for Aerospace Saafety (ARMAS) system, *Space Weather*, doi:10.1002/2016SW001419.
Walker, A. J. (1995), Principles of experimental microdosimetry, *Radiat. Prot. Dosim.*, *61*(4), 297–308.
Waters, M., T. F. Bloom, and B. Grajewski (2000), The NIOSH/FAA working women's health study: Evaluation of the cosmic-radiation exposures of flight attendants, *Health Phys.*, *79*(5), 553–559.
Wilson, J. W., I. W. Joes, D. L. Maiden, and P. Goldhagan (eds) (2003), Analysis, results, and lessons learned from the June 1997 ER-2 campaign, NASA CP-2003-212155, NASA Langley Res. Cent., Hampton, Va.
Wilson, J. W., C. J. Mertens, P. Goldhagan, W. Friedberg, G. D. Angelis, J. M. Clem, K. Copeland, and H. B. Bidasaria (2005), Atmospheric ionizing radiation and human exposure, *Tech. Rep., NASA/TP-2005-213935*, NASA, Washington, D. C.
Wissmann, F., O. Burda, S. Khurana, T. Klages, and F. Langner (2013), Dosimetry of secondary cosmic radiation up to an altitude of 30 km, *Radiat. Prot. Dosim.*, *161*(1–4), 299–302.
Ziegler, J. F., J. P. Biersack, and M. D. Ziegler (2008), The stopping range of ions in solids. [Available at www.SRIM.org.]